



Physico-chemical properties of $\text{MoO}_3/\text{ZrO}_2$ catalysts prepared by dry mixing for isobutane alkylation and butene transformations

Sh.O. Omarov^{a,b}, E.A. Vlasov^{a,b,1}, D.A. Sladkovskiy^{b,c}, K.V. Semikin^{b,c}, A.N. Matveyeva^{a,b}, S.P. Fedorov^{b,c}, G.V. Oganesyan^{b,c}, D.Yu. Murzin^{b,d,*}

^a Department of General Chemical Technology and Catalysis, St. Petersburg State Institute of Technology (Technical University), 26, Moskovsky Ave., St. Petersburg 190013, Russia

^b Laboratory of Catalytic Technologies, St. Petersburg State Institute of Technology (Technical University), 26, Moskovsky Ave., St. Petersburg 190013, Russia

^c Department of Resource-Saving Technologies, St. Petersburg State Institute of Technology (Technical University), 26, Moskovsky Ave., St. Petersburg 190013, Russia

^d Laboratory of Industrial Chemistry and Reaction Engineering, Åbo Akademi University, 8, Biskopsgatan, Turku/Åbo 20500, Finland



ARTICLE INFO

Keywords:

Zirconia
Molybdenum oxide
Porosity
Acidity
Alkylation
Dimerization
Isomerization

ABSTRACT

$\text{MoO}_3/\text{ZrO}_2$ catalysts were prepared either by wet impregnation or tableting dry mechanical mixtures of corresponding zirconium hydroxide and molybdenum containing precursors. It was shown that synthesis parameters influence the phase composition, structure, nature and strength of the acid sites. The structural and textural properties of $\text{MoO}_3/\text{ZrO}_2$ catalysts were characterized by a range of techniques including DTA, XRD, N₂-physisorption, pH-measurements, selective adsorption of a series of acid-base indicators and FTIR spectroscopy of adsorbed pyridine. It is shown that an increase in the concentration of MoO_3 gave a rise to Brønsted acidity concomitant with an increase of 1-butene conversion in isobutane alkylation and butene dimerization. Introduction of up to 6.6% of MoO_3 resulted in sharp changes in physico-chemical properties as well as in catalytic behaviour allowing generation of products with an increased content of C₈ compounds because of alkylation and dimerization. A further increase of MoO_3 content to 13.2% predominantly led to isomerization of 1-butene to 2-butene which can be related to elevated Brønsted acidity.

1. Introduction

Currently one of the ways to improve the properties of gasoline is related to introduction of high octane number additives into motor fuels with poor anti knocking properties. Alkylate with RON above 95 is one of such additives. However, production of alkylate in industry has some apparent deficiencies associated with application of sulfuric or hydrofluoric acids as catalysts [1]. They are notoriously known for equipment corrosion, difficulties with product purification, handling of the spent catalyst and environmental concerns. Not surprisingly there is a strong desire to find suitable heterogeneous catalysts for alkylation. Catalysts based on ZrO_2 and Al_2O_3 have shown high conversion and selectivity. Even more promising are composite materials obtained by additional sulfation of the former oxide [2–5], allowing stabilization of a low temperature tetragonal t- ZrO_2 phase active in alkylation. Presence on the surface of sulfonic and hydrosulfonic groups generates Brønsted acid and Brønsted base centers (denoted as BAC and BBC respectively), while formation of t- ZrO_2 from $\text{ZrO}_{x(\text{OH})_{4-2x}}$ results in Lewis acid centers (LAS). Even if sulfated zirconia based catalysts have high

activity and selectivity towards the desired components – trimethylpentanes, they are prone to deactivation leading to a significant decrease of activity and the product yield [6].

The acidic properties of the catalysts based on zirconia are influenced not only by the presence of sulfonic groups, but also by other compounds, such as for instance WO_3 or MoO_3 . In particular $\text{MoO}_3/\text{ZrO}_2$ catalysts display well defined acid properties [4,7,8,9], moreover molybdenum oxide increases Brønsted acidity [9]. It has been demonstrated that catalysts based on molybdenum and tungsten oxides have shown activity in skeletal isomerization of n-alkanes [10–12]. Catalysts incorporating molybdenum sulfide have found widespread application in various hydrotreating processes [13]. Stabilization of t- ZrO_2 resulting in better resistance to deactivation and higher selectivity in alkylation of isobutane was demonstrated for WO_3/ZrO_2 catalysts [14–16], while for $\text{MoO}_3/\text{ZrO}_2$ similar data are missing, in particular about utilization of molybdenum-heteropolyacids in the synthesis of alkylation catalysts.

It has been reported that $\text{MoO}_3/\text{ZrO}_2$ catalysts displayed catalytic activity in dimerization of alkenes, such as ethylene [8]. Kumar et al.

* Corresponding author at: Laboratory of Industrial Chemistry and Reaction Engineering, Åbo Akademi University, 8, Biskopsgatan, Turku/Åbo 20500, Finland.
E-mail address: dmurzin@abo.fi (D.Y. Murzin).

¹ Deceased.

[17] showed that among different types of β zeolites the highest activity in 1-butene dimerization was exhibited by catalysts with the highest content of Brønsted acid sites, i.e. with a high B/L ratio (0.13 for H- β zeolite). It might be thus expected that $\text{MoO}_3/\text{ZrO}_2$ catalysts with an increased amount of MoO_3 can promote not only dimerization of ethylene, but butenes as well.

The current work is thus devoted to investigation of the influence of various synthesis parameters, namely the type and amount of heteropolyacid as well as treatment temperature on structure, porosity, phase composition and acid-base properties of mixed $\text{MoO}_3/\text{ZrO}_2$ catalysts and their applicability in isobutane alkylation and butene transformations.

2. Experimental

2.1. Catalyst preparation

$\text{MoO}_3/\text{ZrO}_2$ composites were prepared by two different methods, denoted as “wet” and “dry” allowing to explore the influence of the preparation method on catalytic properties. As a precursor for zirconium the following xerogel $\text{ZrO}_x(\text{OH})_{4-2x}$ ($x = 0\text{--}2$) was applied obtained from 10 wt.% ZrOCl_2 (chem. purity) solution by precipitation with 28–30 wt.% solution of NH_4OH (analytical grade) at $\text{pH} \approx 10\text{--}10.5$. The solution of ZrOCl_2 was prepared by dissolving 182.97 g of $\text{ZrOCl}_2\cdot 8\text{H}_2\text{O}$ (101.20 g ZrOCl_2) in distilled water to get the overall mass of the solution equal to 1012 g. This solution was kept at room temperature for 30 min followed by fast addition of 130–135 ml of NH_4OH solution (the acid method). The xerogel was matured for 1 h at room temperature followed by washing from Cl^- ions with a control by AgNO_3 and decanting with water (30 ml per 1 g of ZrOCl_2). After washing the xerogel was filtered using a Nutsche filter and dried at 100–110 °C for 16 h in static air. Obtained xerogel (ca. 70 g calculated as ZrO_2) was used for preparation of 3–4 samples with a different MoO_3 content. The mass losses during calcination (20–700 °C) giving finally $\text{ZrO}_x(\text{OH})_{4-2x}$ were 19.5–23 wt.%.

As Mo containing precursors the following chemicals were used: H_2MoO_4 (analytical grade) denoted as HMo; $\text{H}_4[\text{SiMo}_{12}\text{O}_{40}] \cdot n\text{H}_2\text{O}$ (pure) denoted as HSiMo; $\text{H}_3[\text{PMo}_{12}\text{O}_{40}] \cdot n\text{H}_2\text{O}$ (chem. purity) and $(\text{NH}_4)_6\text{Mo}_7\text{O}_{24} \cdot 4\text{H}_2\text{O}$ (analytical grade) denoted respectively as HPMo and NHMo.

The “wet” series with MoO_3 content 4.2 wt.% were made by wet impregnation of the corresponding xerogel (fraction < 100 μm) with a double excess of HPMo or NHMo water solutions at 70–80 °C, followed by evaporation of the solvent and drying at 100 °C for 3 h. For the “dry” series the influence of MoO_3 content (4.2; 6.6 or 13.2 wt.%) was also investigated. The mixtures of $\text{ZrO}_x(\text{OH})_{4-2x}$ and Mo-containing heteropolyacids were homogenized using sieves below 100 and 40 μm . Thereafter independent on the preparation method the tablets were formed from the corresponding powders using a hydraulic press operating at 130 bar for 120 s. The tablets were then crushed to the fraction 0.8–2 mm and thermally treated according to the following procedure: 100 °C (2 h) \rightarrow 250 °C (1 h) \rightarrow 400 °C (1 h) \rightarrow 500 or 600 or 700 °C (3 h independent on temperature). The synthesized samples are denoted as wt.%Y(i)T, where wt.% correspond to the amount of MoO_3 ; Y – is the type of Mo-containing precursor (HMo; HSiMo, HPMo; NHMo); i – preparation method (D – dry mixing, I – impregnation); T – temperature of the final treatment.

2.2. Catalyst characterization

XRD analysis was done using diffractometer XRD-7000 (Shimadzu) for 20 values 20–40° at 2°/min, using CuK_α as a source and Ni-filter. For analysis of XRD patterns Crystallographica SearchMatchv 1.1 software was applied. The ratio of integral intensities was calculated based on reflexes of the tetragonal t-ZrO₂ – $I_t(101)$ and monoclinic m-ZrO₂ – $I_m(111)$, $I_m(-111)$ phases [18]:

$$X_m = \frac{I_m(111) + I_m(-111)}{I_m(111) + I_m(-111) + I_t(101)} \quad (1)$$

After transformation the volumetric fraction (V_m) of m-ZrO₂ was calculated according to

$$V_m = \frac{PX_m}{1 + (1-P)X_m} 100\% \quad (2)$$

Where

$$P = \frac{H_t(101)}{H_m(111) + H_m(-111)} \quad (3)$$

and H is the reflex intensity. The volumetric fraction (V_t) of tetragonal zirconia t-ZrO₂ is then $V_t = 100 - V_m$.

The constant P in Eq. (2) was assumed to have the value 1.311, as found experimentally by Toraya et al. [18], who determined dependence of V_m from X_m by mixing neat ZrO₂ (99.9%) powder with ZrO₂ ($V_t = 94.8\%$) powder, precipitated from the gas phase and containing amorphous SiO₂.

The size of t-ZrO₂ was calculated based on the Scherrer equation, reflecting reciprocal dependence of the crystal size on the width of the peak at half height.

Thermogravimetry and DTG analysis was done with DTG-60A (Shimadzu). A sample of ca. 20.0 ± 0.20 mg was calcined in air with a temperature ramp 10°/min. The error of weight measurements was 1% and 1 μV for DTA.

Nitrogen physisorption was conducted with Autosorb 6iSA (Quantachrome) at 77 K. The surface area was calculated using the multi-point Brunauer-Emmett-Teller (BET) method, while the pore sizes were assessed applying the Barret-Joyner-Halenda method.

For overall surface acidity and basicity, elucidation of the Hammett acidity functions was done following the previous work of the authors [5,19]. In particular, adsorption of various indicators covering a broad range of pK_a from –4.4 to 14.2, was investigated. Such indicators adsorb selectively on different types of Brønsted and Lewis acid and base centers [19]. Concentration of various centers can be calculated by monitoring the optical density of water solutions of these indicators. In this work this was done using a spectrophotometer SF-46. In addition, adsorption of pyridine was applied to quantify the acid sites. To this end pyridine was adsorbed on the catalyst samples (20–30 mg) at 20 °C, followed by thermal desorption at 150, 250 and 350 °C. The amount of retained pyridine was elucidated by FTIR [20] using IrTracer-100 (Shimadzu) spectrophotometer. The ratio between BAS to LAS (B/L) was calculated taking into account the integral intensity and extension coefficients of pyridine adsorption on respective sites [20].

2.3. Catalytic experiments

The experimental setup for alkylation of isobutane with C₄ olefin mixture is shown in Fig. 1.

A once-through plug-flow reactor (8 mm diameter, 20 cm length) was used with the catalyst loading of 7 cm³. The feedstock was prepared by mixing isobutane from KINEF refinery (Russia) and an olefin, which was produced by butanol dehydration. The feedstock composition was: 90.7% isobutane; 5.8% 1-butene; 1% *trans*-butene-2; 2% *cis*-butene-2; 0.5% n-butane and 80 ppmw of propylene, propane and butyne. Prior to the reaction, the catalysts were dried ex situ at 350°C for 2 h under air. The following reaction conditions were used: 17 barg, 80°C, isobutane to C₄-olefin ratio of 10:1, olefin space velocity 0.6 gbuten/g_{cat}·h. The reactor effluent was cooled down to room temperature and collected in a separator. The liquid samples were taken periodically (every 30 min) through a pressurized sampling loop and stored at -18°C prior to GS analysis. The separator was emptied after each sample. Therefore, each product composition represents an averaged catalyst activity during the sampling time. A back pressure regulator was used to sustain the pressure. Analysis of the products were done

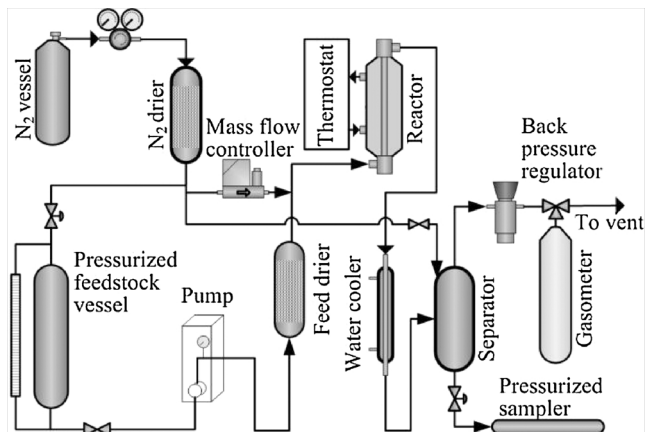


Fig. 1. Schematic diagram of the continuously operated alkylation of isobutane with butenes.

using the gas chromatograph Shimadzu GC-2010 Plus equipped with a flame ionization detector and a capillary column (Supelco Petrocol, 100 m, $di = 0.25$ mm, stationary phase: polydimethylsiloxane, carrier gas: helium. Temperature program: 35 – 60°C heating at rate 1°C/min and 60 – 200°C heating with 10°C/min rate for C_{9+} hydrocarbon determination). Conversion of 1-butene (X) was calculated as the amount of reacted C_4 -olefin related to the initial concentration, while selectivity was evaluated based on C_{5+} hydrocarbons distribution in the reactor effluent.

Potential impact of internal diffusion limitations was assessed using the Weisz-Prater criterion. The Weisz-Prater modulus was calculated for the mean radius of the catalyst particles of 0.7 mm, maximal initial reaction rate and the mean substrate concentration. Equation of Wilke-Chang was used for calculation of the diffusion coefficient of 1-butene in isobutane. A conservative ratio between the catalyst porosity and tortuosity equal to 0.1 was assumed in estimation of the effective diffusion coefficient. The estimated Weisz-Prater modulus for the second order reaction was very close to the value below which the absence of pore diffusion limitations is typically considered. Taking into account several assumptions in calculations of the Weisz-Prater modulus in the current work some influence of internal mass transfer limitations cannot be, however, completely ruled out.

To describe the product composition six main reaction routes can be considered which include reactions typical for alkylation of isobutane by 1-butene or 2-butene and its dimerization:

- 1) Olefin isomerisation: $1\text{-butene} \leftrightarrow \text{cis}\text{-butene-2} \leftrightarrow \text{trans}\text{-butene-2}$
- 2) Alkylation: $C_4H_{10} + C_4H_8 \rightarrow C_8H_{18}$ (trimethylpentanes, dimethylhexanes)
- 3) Dimerization: $2 \cdot C_4H_8 \rightarrow C_8H_{16}$ (octene isomers)
- 4) Multiple alkylation: $C_8H_{18} + C_4H_8 \rightarrow C_{12}H_{26}$
- 5) Oligomerisation: $C_8H_{16} + C_4H_8 \rightarrow C_{12}H_{24}$
- 6) Cracking of C_{9+} hydrocarbons

The results of catalytic experiments were compared on the basis of selectivity to the reaction products and 1-butene conversion. The conversion was calculated according to

$$X = (n_{1-C4\text{in}}^{in} - n_{1-C4\text{out}}^{out}) / n_{1-C4\text{in}}^{in} \quad (4)$$

where $n_{1-C4\text{in}}^{in}$, $n_{1-C4\text{out}}^{out}$ molar flows of 1-butene in the feed and in the liquid product, [mole/h].

The gaseous products are not included in calculations of conversion and selectivity due to negligible yields of hydrocarbons in the gas phase. In fact, approximately 98% of hydrocarbons were present in the liquid product while only minor amounts of propane products were detected, which can be explained by mild reaction conditions not favourable for cracking.

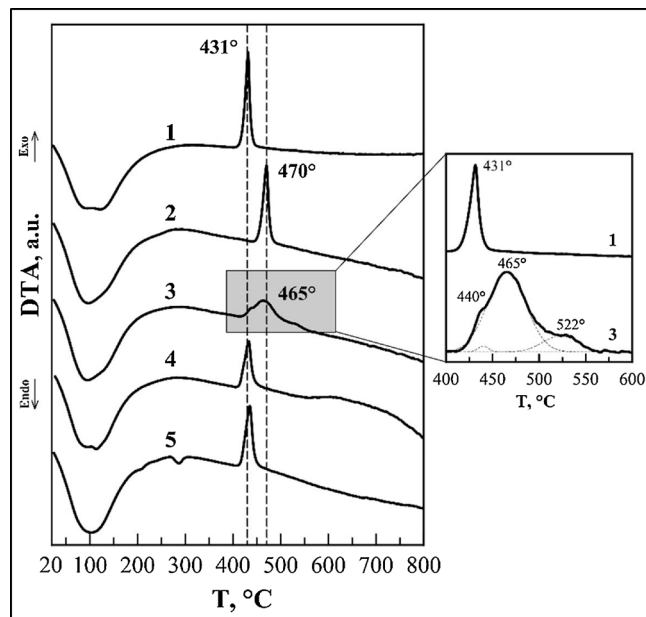


Fig. 2. DTA curves for samples, containing 4.2 (2, 3, 5) and 13.2 (4) wt.% MoO_3 , obtained by impregnation (2, 3) and dry mixing (4, 5) from NHMo (2, 5) and HPMo (3, 4); $ZrO_x(OH)_{4-2x}$ (1).

Selectivity for isomerization S_{iso} , alkylation S_A and dimerization S_D was defined as the molar flows of respectively 2-butenes, C_8 -alkanes and total isoctenes C_{08} at the reactor output corrected by the stoichiometric coefficient of alkylation and dimerization equal to 2

$$S_{iso} = (n_{2-C4\text{in}}^{out} - n_{2-C4\text{in}}^{in}) / (n_{1-C4\text{in}}^{in} - n_{1-C4\text{in}}^{out}) \quad (5)$$

$$S_A = 2n_{i8}/(n_{1-C4\text{in}}^{in} + n_{2-C4\text{in}}^{in} - n_{1-C4\text{in}}^{out} - n_{2-C4\text{in}}^{out}) \quad (6)$$

$$S_D = 2n_{08}/(n_{1-C4\text{in}}^{in} + n_{2-C4\text{in}}^{in} - n_{1-C4\text{in}}^{out} - n_{2-C4\text{in}}^{out}) \quad (7)$$

where n_{i8} and n_{08} – molar flows of C_8 alkanes or C_8 olefins respectively, [mole/h].

The cracking ratio was defined as the amount of $C_5\text{-}C_7$ products to the total C_{9+} oligomerisation/multiple alkylation products.

3. Results and discussion

3.1. DTA-TGA

During thermal decomposition of $ZrO_x(OH)_{4-2x}$ two endothermal effects are visible from DTA (Fig. 2), connected to removal of adsorbed on the surface and chemically bound water located in the interlayers of amorphous ZrO_2 . According to the thermal analysis and XRD an increase of temperature up to 400 °C is accompanied by removal of a small amount of water and a decrease in the lattice parameters of t-ZrO₂. The exoeffect of amorphous ZrO_2 crystallisation is seen at 431 °C, while some minor endoeffects can be ascribed to decomposition of the molybdenum containing compounds present initially.

Fig. 2 illustrates that crystallization of ZrO_2 depends on the preparation method, heteropolyacid type and MoO_3 content, influencing the final phase composition and texture of MoO_3/ZrO_2 catalysts.

For 4.2NHMo(I) and 4.2HPMo(I) samples obtained by impregnation of xerogel with ammonium paramolybdate and phosphomolybdenic acid, crystallization of ZrO_2 starts at a higher temperature of 470 and 462 °C (curve 2 in Fig. 2), compared to $ZrO_x(OH)_{4-2x}$ and a sample of the same composition 4.2NHMo(D) obtained by dry mixing (curve 1, Fig. 2) with the respective temperature being equal to 431 °C. It can be suggested that the difference in the crystallization temperature is related to a more effective blocking of ZrO_2 crystallites by $[Mo_7O_{24}]^{6-}$.

and $[\text{PMo}_{12}\text{O}_{40}]^{3-}$ adsorbed from the solution compared to the samples formed by mechanical mixing of the xerogel with $(\text{NH}_4)_6\text{Mo}_7\text{O}_{24}$ and $\text{H}_3[\text{PMo}_{12}\text{O}_{40}]$. A similar effect was reported in [21] after incorporation of MoO_3 by impregnation from $(\text{NH}_4)_6\text{Mo}_7\text{O}_{24}$, when the exothermal crystallization of samples obtained by impregnation and containing 1.0 wt.% MoO_3 , was seen at 484 °C. 4.2H₂PMo(I) displayed a specific behaviour compared to 4.2NHMo(I), namely several overlapping exo-effects in the region of amorphous ZrO_2 crystallization (440, 465 and 522 °C). The results obtained by López-Salinas et al. [22], as well as Devassy et al. [23,24], for 12-tungstophosphoric acid supported on $\text{Zr}(\text{OH})_4$ have demonstrated that different types of interactions between the anion in HPA and the dehydrated form of zirconium hydroxide can be present in the temperature region 400–600 °C. Based on the literature data [22–24] it can be suggested that the first exoeffect at (440 °C) can be either related to interactions of the surface $\text{Mo} = \text{O}$ groups and $=\text{Zr}^+$ with formation of $\text{Zr}-\text{O}-\text{Mo}$ bonds or removal of protons from HPA because of their interactions with $\text{Zr}-\text{OH}$. Stronger interactions of ZrO_2 with HPA are the origin of the second exo-effect at 465 °C reflecting partial crystallization of dehydrated amorphous ZrO_2 . Interpretation of the third exo-effect at (522 °C) is more challenging, however, it can be tentatively proposed that this effect corresponds to destruction of HPA anions giving MoO_3 and phosphate ions, as well as to completion of ZrO_2 crystallization upon influence of HPA decomposition products.

For samples obtained by mixing and containing 13.2 wt.% MoO_3 , TG curves for the temperature region 400–800 °C are displayed in Fig. 3. Below 400 °C only losses of physically and chemically bound water were seen along with partial decomposition of HPA. As can be seen after 700 °C there is a minor mass loss (0.30–0.35 wt.%), which can be attributed most probably to sublimation of molybdenum oxide. It should be noted that this effect was seen only for MoO_3 content equal to 13.2%, while TG-curves for samples with 6.6 wt.% MoO_3 (not shown) did not display any mass loss. The role of molybdenum oxide lability with an increase of treatment temperature during solid phase synthesis can be explained by the solid-solid wetting, (SSW) which will be discussed in Section 3.3.

3.2. Phase composition

XRD patterns for catalysts prepared by impregnation contained, independent on the nature of the solution, intensive lines (Fig. 4) attributed to t- and m- ZrO_2 , while a weak reflex at $2\theta = 27.28^\circ$ is

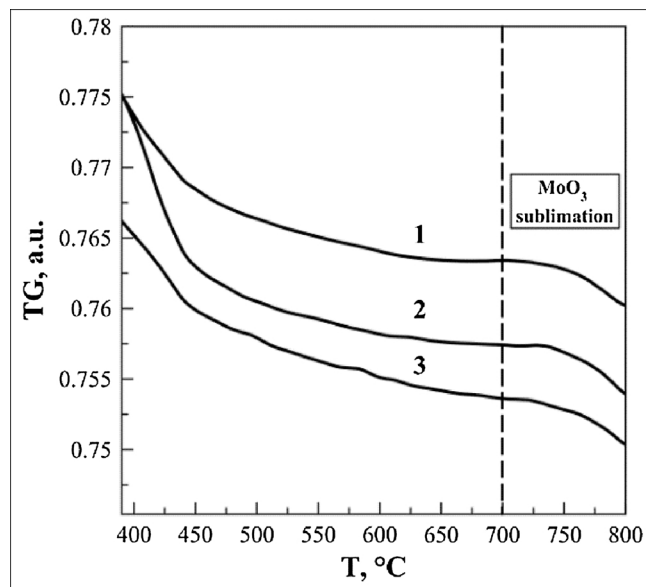


Fig. 3. TG-curves for samples 13.2XMo (X = H (1); Si (2); P (3)) made by dry mixing.

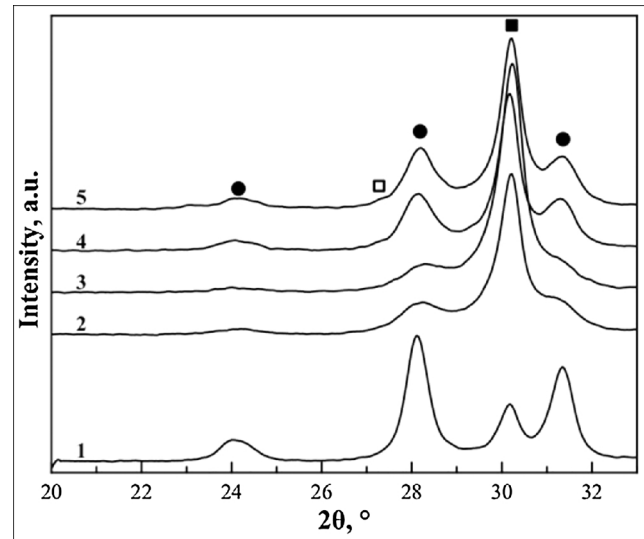


Fig. 4. XRD for samples containing 4.2 wt. % MoO_3 and obtained by impregnation (2, 3) and dry mixing (4, 5) from HPMo (2, 4) and NHMo (3, 5) at 600 °C; ZrO_2 -600 (1); (• - m- ZrO_2 ; ■ - t- ZrO_2 ; □ - o- MoO_3).

characteristic for o- MoO_3 . During impregnation of the xerogel, solutions containing Mo fill the pore volume. $[\text{MoO}_4]^{2-}$ and $[\text{PMo}_{12}\text{O}_{40}]^{3-}$ -anions are adsorbed also on the outer surface of the dispersed particles, blocking crystals of t- ZrO_2 formed after crystallization. MoO_3 formed in the pores during thermal treatment is probably only mildly crystalline.

Nature of Mo-containing precursor had an influence on the phase composition of catalysts made by dry mixing when the concentration of MoO_3 and calcination temperature were elevated (Fig. 4 and Table 1). Thus the o- MoO_3 phase was seen after thermal treatment at 500 °C for all types of molybdenum heteropolyacids (6.6–13.2 wt. % MoO_3), while the same holds only for 6.6 HMo(D) when treated at 600 °C.

For other $\text{MoO}_3/\text{ZrO}_2$ catalysts synthesized from heteropolyacids and molybdenic acid there was a phase transition between from o → m- MoO_3 when the temperature was elevated from 500 to 600 °C. In the case of the maximum amount of MoO_3 used in the current work (13.2 wt.%) for all heteropolycompounds of molybdenum applied in the synthesis (700 °C) it was possible to see reflexes attributed to h-Zr (MoO_4)₂ phase. Moreover, zirconium molybdate was observed for 13.2H₂PMo(D) treated at 600 °C. It should be noted that presence of h-Zr (MoO_4)₂ phase for samples with 15 wt. % MoO_3 , prepared by impregnation was seen only after treatment at 700 °C [25,21].

Transformation of low temperature metastable t- ZrO_2 phase into thermodynamically stable m- ZrO_2 phase occurs in parallel to phase transformation of MoO_3 . Thus at 600 °C the volume fraction of t- ZrO_2 phase obtained by thermal treatment of $\text{ZrO}_x(\text{OH})_{4-2x}$ is only 13.8% (Table 2) in agreement with the literature data [26]. Upon introduction of MoO_3 either by dry mixing or impregnation there are substantial changes during the structural transformation mentioned above.

When the thermal treatment temperature was increased in the

Table 1
Changes of the phase composition.

MoO_3 , wt. %	T, °C			
		500	600	700
4.2	t- and m- $\text{ZrO}_2 + \text{o-}\text{MoO}_3$	t- and m- $\text{ZrO}_2 + \text{o-}\text{MoO}_3$	–	–
6.6	t- and m- $\text{ZrO}_2 + \text{o-}\text{MoO}_3$	t- and m- $\text{ZrO}_2 + \text{o-}\text{MoO}_3$	t- and m- $\text{ZrO}_2 + \text{m-}\text{MoO}_3$	t- and m- $\text{ZrO}_2 + \text{m-}\text{MoO}_3$
13.2	t- and m- $\text{ZrO}_2 + \text{o-}\text{MoO}_3$	t- and m- $\text{ZrO}_2 + \text{m-}\text{MoO}_3$	t- and m- $\text{ZrO}_2 + \text{m-}\text{MoO}_3$	t- and m- $\text{ZrO}_2 + \text{m-}\text{MoO}_3 + \text{h-Zr}(\text{MoO}_4)_2$

Table 2

Volume fraction of the phase V_t and its size (in parenthesis, nm) in $\text{MoO}_3/\text{ZrO}_2$ samples depending on the precursor type and calcination temperature.

Catalyst Notation	MoO ₃ , wt.%	Precursor	T, °C			
			500	600	700	
ZrO ₂	–	–	60.4 (17.7)	13.8 (13.1)	6.0 (8.7)	
H ₂ SiMo(D)	6.6	H ₄ [SiMo ₁₂ O ₄₀]·nH ₂ O	67.6 (15.7)	75.4 (17.0)	53.6 (15.7)	
	13.2		81.1 (15.5)	92.2 (17.5)	83.5 (17.9)	
HPMo(I)	4.2	H ₃ [PMo ₁₂ O ₄₀]·nH ₂ O	62.7 (13.1)	59.1 (13.5)	36.7 (14.3)	
HPMo(D)	6.6		48.0 (16.0)	46.8 (15.4)	34.2 (14.8)	
	13.2		41.4 (15.0)	67.1 (15.6)	41.6 (16.3)	
HM(D)	6.6	H ₂ MoO ₄	71.4 (15.3)	86.5 (17.0)	76.8 (17.6)	
	13.2		53.2 (15.3)	69.3 (15.7)	–	
NHMo(I)	4.2	(NH ₄) ₆ Mo ₇ O ₂₄ ·4H ₂ O	78.3 (14.4)	86.8 (15.8)	84.5 (15.5)	
NHMo(D)			78.5 (14.3)	77.7 (14.4)	53.4 (16.4)	
			49.1 (14.0)	49.2 (14.3)	34.1 (14.5)	

sequence: 500→600→700 °C, practically for all samples made by dry mixing there was a maximum V_t (minimum V_m) at 600 °C (Table 2), which is probably related to the size effect. Up to 500 °C there is formation and growth of t-ZrO₂ crystals, which after reaching a certain size (30 nm according to [27]) start to be transformed into m-ZrO₂. This process is seen as an increase in the fraction of the m-ZrO₂ phase. At 600 °C molybdenum oxide located on the surface of t-ZrO₂ crystals, being itself in a weakly crystalline state (Fig. 4), prevents growth of these crystals and slows down transformations from t-ZrO₂ to m-ZrO₂, thereby maintaining an elevated fraction of t-ZrO₂. Such behaviour was most prominent when HSiMo was used in the synthesis of catalysts by dry mixing, for the case of NHMo utilization by impregnation (Table 2) as well as for all heteropolyacids with the highest MoO₃ (13.2 wt.%) loading. Nevertheless when 700 °C was reached there was no stabilization anymore leading to a sharp increase of m-ZrO₂ content independent on the preparation method and HPA type.

It should be noted that the structural transformations t→m-ZrO₂ with temperature increase in the sequence 500→600→700 °C do not lead to changes in the size of zirconia for MoO₃/ZrO₂ catalysts ($d = 14\text{--}17$ nm), while thermal treatment of ZrO_x(OH)_{4-2x} gives a two-fold decrease in the size from 17.7 to 8.7 nm.

A low amount of t-ZrO₂ in 4.2–6.6HPMo(D) is connected with the total destruction of phosphormolybdenum acid structure occurring above 500 °C [28], and agglomeration of the dispersed MoO₃ crystals above 600 °C into large agglomerates which cannot effectively block t-ZrO₂ crystals (Table 2).

It can be thus concluded that introduction of MoO₃ in the form of different precursors allows to slow down sintering of ZrO₂ and to increase thermal stability of a metastable t-ZrO₂ phase [29], whose presence is required to ensure catalytic activity of zirconia in isobutane alkylation [2–4]. The experimental data in the current work demonstrate that the most prominent effect of t-ZrO₂ stabilization was achieved utilizing HSiMo as a precursor for the catalyst prepared by dry mixing (Fig. 5).

3.3. Porous structure

According to the adsorption isotherms (Fig. 6) the synthesized materials belong to type IV (BDDT classification [30]). Changes in the hysteresis loop with temperature increase were attributed by de Boer to transformations of the slit like pore (type B) to the wedge type (type C) [30].

All MoO₃/ZrO₂ catalysts have a bimodal porous structure (Table 3). The same structure of porosity was reported in [26] for ZrO₂ obtained by thermal treatment of ZrO_x(OH)_{4-2x} although the type of pores was different, namely dead end (hysteresis type E) and cylindrical pores (type A) were present.

There was practically no influence of the precursor nature and MoO₃ content for samples obtained by dry mixing on the predominant

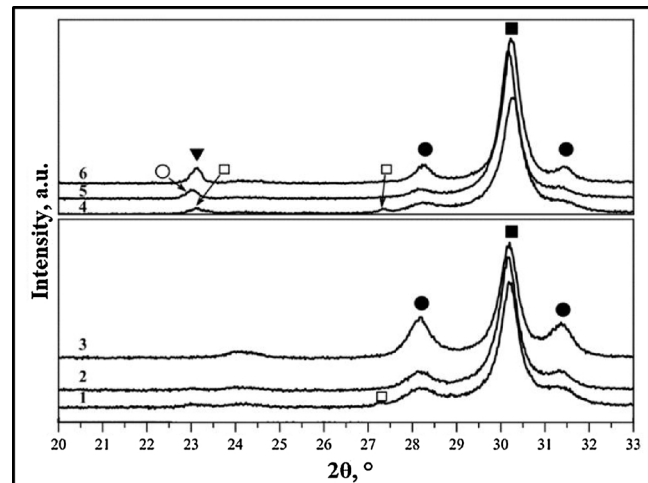


Fig. 5. XRD of samples containing 6.6 (1–3) and 13.2 (4–6) wt.% MoO₃, obtained by dry mixing from HSiMo and treated at 500 °C (1, 4), 600 °C (2, 5) and 700 °C (3, 6). (● – m-ZrO₂; ■ – t-ZrO₂; ○ – m-MoO₃; □ – o-MoO₃; ▼ – Zr(MoO₄)₂).

mesopore size as in all cases there were small (3–4 nm) and larger mesopores (6–10 nm, Table 3). At the same time elevation of the treatment temperature from 400 to 600 °C leads to a decrease of the specific surface area, the mesopore volume and simultaneously to an increase of the diameter of large pores because of more prominent catalyst sintering.

Comparison of ZrO₂ texture with the porous structure of the samples on the basis of phosphormolybdenum acid prepared either by dry mixing 4.2HPMo(D) or impregnation 4.2HPMo(I) (600 °C, Table 3) reveals a finer structure for the catalysts obtained by impregnation (26, 57 and 86 m²/g, respectively), and blocking of dispersed t-ZrO₂ crystallites by MoO₃ is more efficient in the case of impregnation than in the case of catalysts prepared by dry mixing.

With an increase of the treatment temperature the specific surface area of ZrO₂ and MoO₃/ZrO₂ is decreasing (Fig. 7) independent on the synthesis method, moreover dependence of specific surface area as a function of temperate correlated well with DTA. Thus, for samples obtained by dry mixing and impregnation, a sharp decrease in the specific surface area was seen for the temperature interval of ZrO₂ crystallization. This was related to substantial structural changes, namely above 400 °C for samples made by dry mixing and for impregnation samples respectively in the intervals 500–600 °C for 4.2NHMo(I) and 600–700 °C for 4.2HPMo(I) (Fig. 7). Higher values of specific surface area for 4.2NHMo(I) and 4.2HPMo(I) below 500–600 °C in comparison with the samples synthesized by dry mixing can be explained by the presence of amorphous ZrO₂. This is also in line with XRD patterns for the sample treated at 600 °C.

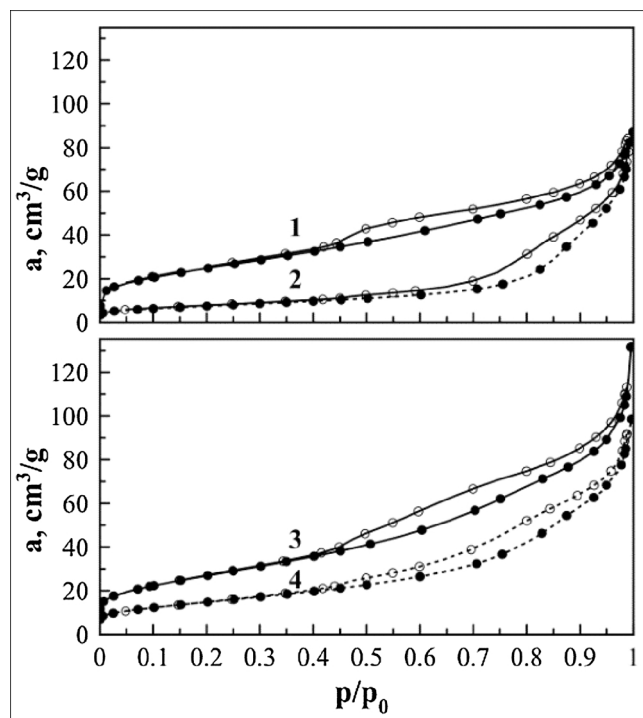


Fig. 6. Nitrogen adsorption-desorption isotherm for ZrO₂ (1,2) and 6.6HSiMo(D) (3,4), thermally treated at 400 (1,3) and 600 °C (2,4) (• – adsorption curve; ○ – desorption curve).

Comparison of data for the catalysts obtained by dry mixing reveals that HSiMo samples possess the best textural characteristics in terms of potential catalytic performance, as a combination of large (ca. 8 nm size) and smaller mesopores (ca. 3 nm) can diminish diffusional limitations during alkylation in comparison with catalysts with smaller pores.

Summarizing the results mentioned above it is worth to discuss the solid-solid wetting, which was described in [28,29,31,32] for MoO₃/ZrO₂ catalysts prepared by mixing individual oxides with subsequent calcination at 800 °C. The solid-solid wetting results in a monolayer of molybdenum oxide on zirconia. This effect was demonstrated for treatment at 800 °C and a high content of MoO₃, which was confirmed by XRD and surface area measurements revealing a maximum of specific surface area for 12 wt.% MoO₃ and 800 °C.

A similar effect was observed in the current work albeit at lower temperatures ~600 °C. Thus according to XRD for samples with 6.6 wt. % MoO₃ treated at 600–700 °C there were no reflexes of molybdenum oxide phase as well as of the bulk phase of zirconium molybdate. When

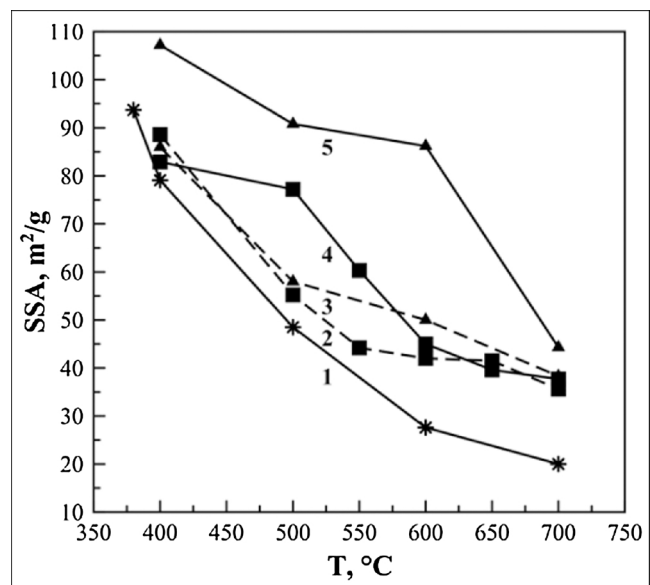


Fig. 7. Changes of specific surface area vs thermal treatment temperature for MoO₃/ZrO₂ samples, containing 4.2 wt.% MoO₃ and obtained by dry mixing (2,3) and impregnation (4,5) from NHMo (2,4) and HPMo (3,5); ZrO₂ (1).

the content of MoO₃ increased to 13.2%, it was possible to observe the reflexes of m-MoO₃ for the treatment at 600 °C, while zirconium molybdate started to be seen for the sample treated at 700 °C. Surface area measurements (Table 3) illustrate a sharp increase of the specific surface area up to 6.6 wt.% MoO₃ and a minor increase of it from 6.6 to 13.2% MoO₃ independent of Mo-precursor. Behaviour of V_t with an increase of MoO₃ content was similar. Such dependences of V_t and specific surface area, namely an increase up to 6.6 wt.% MoO₃, point out on the presence of solid-solid wetting influencing significantly formation of the final MoO₃/ZrO₂ structure. Sharp changes in the properties of MoO₃/ZrO₂ systems when MoO₃ content is increasing to 6.6 wt.% are in line with the literature data [34] generated by deposition of MoO₃ from ammonium paramolybdate on monoclinic ZrO₂.

It should be noted that at 6.6 wt.% MoO₃ its surface density is close to 5 Mo atoms/nm² (Table 3), in agreement with conclusions of Afanasiev [29] that a monolayer coverage of molybdenum oxide is a metastable phase, which can be obtained from different initial states depending on the precursor and pretreatment. In the current work tabletting using a hydraulic press resulted in an intimate contact of the starting components with respect to each other allowing therefore adequate interactions during thermal treatment.

Table 3

Influence of synthesis parameters (Mo-precursor, calcination temperature and MoO₃ contain) on porous structure MoO₃/ZrO₂ systems.

Catalyst	T, °C	Textural characteristics			
		Notation	MoO ₃ , wt.%	V _{mes} , cm ³ /g	S, m ² /g
ZrO ₂	–	400	0.13	87	0
	–		600	0.13	26
HPMo(I)	4.2	400	0.16	86	2.04
	–		600	0.16	3.08
HPMo(D)	6.6	400	0.18	95	2.90
	–		600	0.15	5.31
HSiMo(D)	13.2	400	0.18	59	9.36
	–		600	0.13	3.37
	–		600	0.13	45
HPMo(D)	6.6	400	0.14	82	6.13
	–		600	0.14	58
HM(D)	13.2	400	0.14	58	9.52
	–		600	0.13	4.60
HM(D)	6.6	400	0.13	60	9.36
	–		600	0.14	59

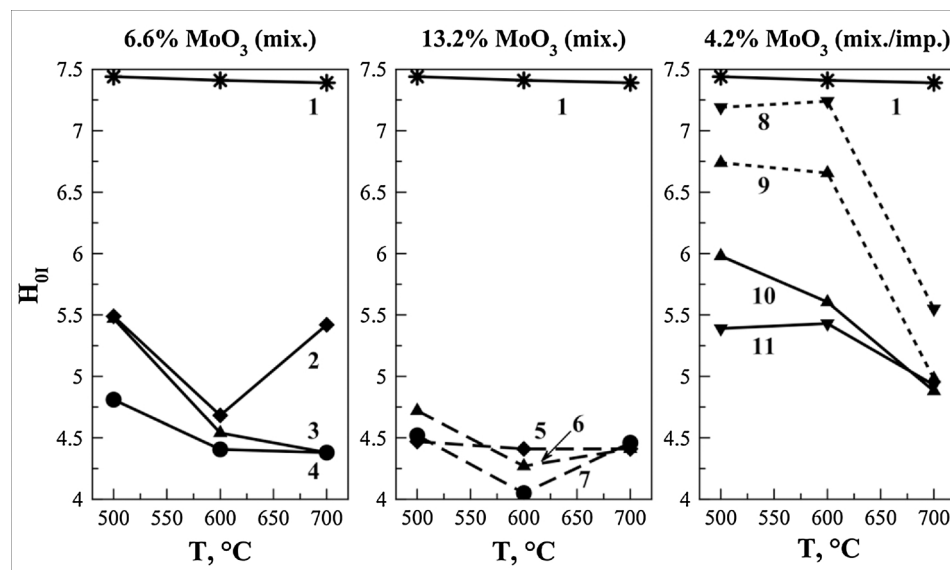


Fig. 8. Dependence of Hammett function on calcination temperature for ZrO_2 (1) and $\text{MoO}_3/\text{ZrO}_2$ samples obtained by dry mixing (2–7, 10, 11) and impregnation (8, 9) and containing 4.2 (8–11), 6.6 (2–4) and 13.2 (5–7) wt.% MoO_3 from HMo (2, 5); HPMo (3, 6, 9, 10); HSiMo (4, 7) and NHMo (8, 11).

3.4. Acidity

Surfaces of all $\text{MoO}_3/\text{ZrO}_2$ catalysts possess acidic properties clearly increasing with elevation of MoO_3 content as can be seen from changes of the integral Hammett function (H_{01} , Fig. 8). For the sake of comparison Table 4 contains values of H_0 for a range of several acid catalysts: zeolites NaY, HY, NaX, CaX; $\text{ZrO}_x(\text{OH})_{4-2x}$ sulphated with $(\text{NH}_4)_2\text{SO}_4$ solution based on 9% SO_4^{2-} loading and thermally treated at 600 °C ($\text{SO}_4^{2-}/\text{ZrO}_2$). In addition, the data of Tanabe [33] for MgO, ZnO and ZnS are also given.

Most probably the character of $H_{01}=f(T)$ function for the samples made by dry mixing having a minimum at 600 °C, can be explained by phase transitions o→m- MoO_3 occurring at 500–600 °C. In addition, it can be related to completion of hydrate layer formation because of decomposition of the initial Mo containing acids. At the current moment it is difficult to fully explain an increase of acidity in the temperature range 500–600 °C for the samples made by dry mixing. In the temperature range 600–700 °C behaviour of these catalysts is similar to $\text{MoO}_3/\text{ZrO}_2$ materials prepared by impregnation. El-Sharkawy et al. [27] using TPD of ammonia demonstrated that independent on MoO_3 content a decrease of surface acidity for $\text{MoO}_3/\text{ZrO}_2$ for thermal treatment above 550 °C can be explained by formation of surface Mo-O-Zr bonds by precursors of zirconium molybdate. A similar behaviour for impregnated catalysts was observed by Zhao et al. [35] and Yori et al. [12].

For the catalysts made by impregnation a sharp decline in H_{01} with a calcination temperature increase can be explained by a decline in the number of tightly bound OH-groups (curves 8 and 9 in Fig. 8).

Application of phosphormolybdenum acid for preparation of $\text{MoO}_3/\text{ZrO}_2$ catalysts by impregnation and silicon-molybdenum acid in dry mixing allows to achieve more acidic surfaces because of a larger number of protons in these precursors. To get additional information about acidity and acid sites on the surface the samples made by impregnation and dry mixing with HSiMo were studied by pyridine FTIR and adsorption of indicators.

Table 4
Integral Hammett function [19,33] for acid and base catalysts.

Material	MgO	ZnO	ZnS	CaX	NaX	NaY	HY	$\text{SO}_4^{2-}/\text{ZrO}_2$
H_{01}	10.8	6.9	5.0	10.9	12.5	11.2	8.3	3.2

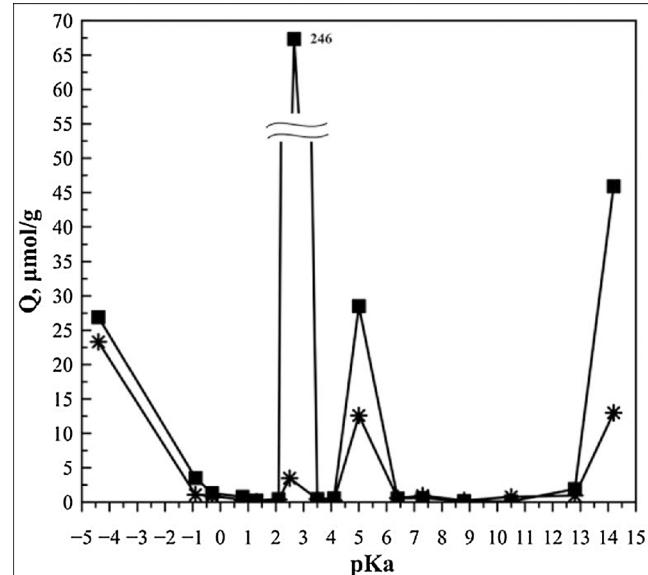


Fig. 9. Distribution of adsorption centers on the surfaces of ZrO_2 (*) and MoO_3 (■).

Figs. 9–11 reflecting acidity of the studied catalysts by adsorption of indicators reveal that MoO_3 , made by thermal treatment of silicon molybdenum acid at 600 °C in comparison to ZrO_2 (Fig. 9) has a higher concentration of Brønsted acid centers (BAS). Such BAS corresponding to hydroxyl groups with different special arrangement lead to low values of H_0 . At the same time Lewis acid centers ($pK_a = 14.2$) and weak BAS ($pK_a = 5$) are present on the surfaces of both oxides (Fig. 9). Mixing of precursors followed by thermal treatment and subsequent sintering result in the catalyst structure with various functional groups.

Dry mixing approach for making samples with up to 6.6 wt.% MoO_3 in a mixture with zirconia xerogel results in a sharp decrease of strong BAS with $pK_a = 2.5$, being predominant on the surface of molybdenum oxide and representing OH-Mo species. In the case of higher MoO_3 loading (13.2 wt.%) there is a substantial redistribution of the type and strength of acid sites, thus concentration of BAS with $pK_a = 2.5$ is decreasing 7–8 fold, while concentration of LAS with $pK_a = 14.2$ (cations Zr^{4+} , Mo^{6+} , Si^{4+} , P^{5+}) and BAS with $pK_a = 5.0$ (hydrated bridged O atoms) is increasing 16–17 and 10–11 fold respectively.

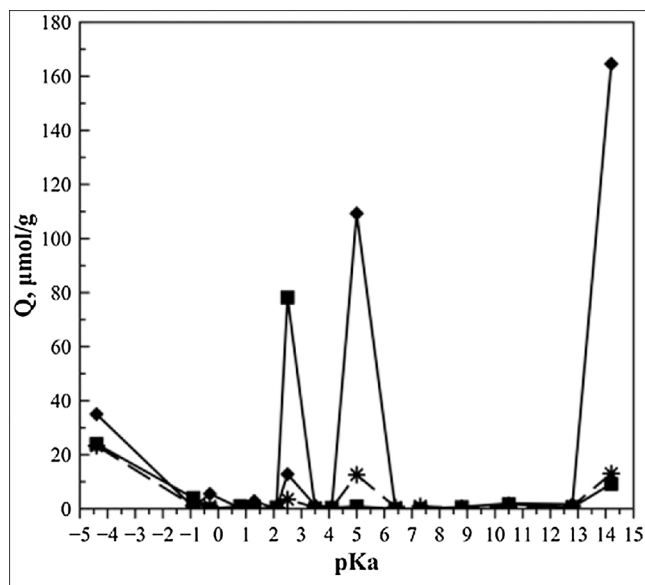


Fig. 10. Distribution of adsorption centers on the surfaces of ZrO_2 (*) and $\text{MoO}_3/\text{ZrO}_2$ obtained by dry mixing from HSiMo , treated at 600°C and containing 6.6 (■) and 13.2 (◆) wt.% MoO_3 .

Changes in the surface acidity of $\text{MoO}_3/\text{ZrO}_2$ are related to the mutual influence of Mo, Zr and Si oxides (Fig. 10). Most probably active acidic OH groups with $\text{pKa} = 2.5$, located on the surface of MoO_3 , can enhance Lewis acidity of coordinatively unsaturated surface cations Zr^{4+} and Mo^{6+} because of element – oxygen bridging bonds with hydroxyl groups which are adsorbed on these cations. It cannot be ruled out that an increase in the concentration OH-groups with $\text{pKa} 5.0$ is related to the presence of SiO_2 in the silicon containing precursor. Silica *per se* does not have practically any hydroxyl groups on the surface. However, in the silicon-molybdate ion hydrogen is connected to the bridge oxygen in Mo-O-Si and upon thermal treatment hydroxyl groups can be formed not only on the surface of molybdenum oxide, but also on silica. Another argument in favour of surface hydroxyl group on silica is based on the suggestion of an intimate contact of the acid precursor with $\text{ZrO}_x(\text{OH})_{4-2x}$, with transfer of -OH groups to silica during calcination.

Preparation of the catalysts by impregnation and thermal treatment at 600°C also ensures presence of various acid-base sites on the surfaces (Fig. 11). An increase of Lewis and Brønsted acidity is visible upon introduction of MoO_3 . In particular LAS ($\text{pKa} = 14.2$), strong ($\text{pKa} = 2.5$) and weak ($\text{pKa} = 5.0$) BAS, as well LBS with $\text{pKa} = -4.4$ (because of oxygen in $\text{Zr} = \text{O}$ and $\text{Mo} = \text{O}$) along with a small amount of BBS with $\text{pKa} = -0.8$ and -0.3 (bridging oxygen atoms with $\text{Zr}-\text{O}-\text{Zr}$, $\text{Zr}-\text{O}-\text{Mo}$ and $\text{Mo}-\text{O}-\text{Mo}$) are present. Thereby introduction of heteropolycompounds of molybdenum increases concentration of LAS decreasing at the same time overall concentration of BAS and basic sites in line with the data reported in the literature [36] and can point out on formation of vacant and electron deficient LAS because of dehydration. In order to assess the quantity and strength of acid sites made by impregnation and dry mixing using ammonium para molybdate and silicon molybdenum acid an analysis by pyridine FTIR was also performed (Figs. 12–15).

In the spectra of the samples made by impregnation (Fig. 12) vibration frequencies of pyridine adsorbed on strong LAS (type 19b at 1444 cm^{-1}) are present [22]. Vibration frequencies at 1575 and 1595 cm^{-1} correspond to weak LAS [22]. A low intensity of vibrations attributed to type 19a (1490 cm^{-1}) from $\text{C}_5\text{H}_5\text{NH}^+$ and 19b (1540 cm^{-1}) from pyridine on BAS indicates a low amount of BAS on the surface in agreement with the analysis made with indicators (Fig. 11). The nature of Lewis acidity for ZrO_2 -containing systems is

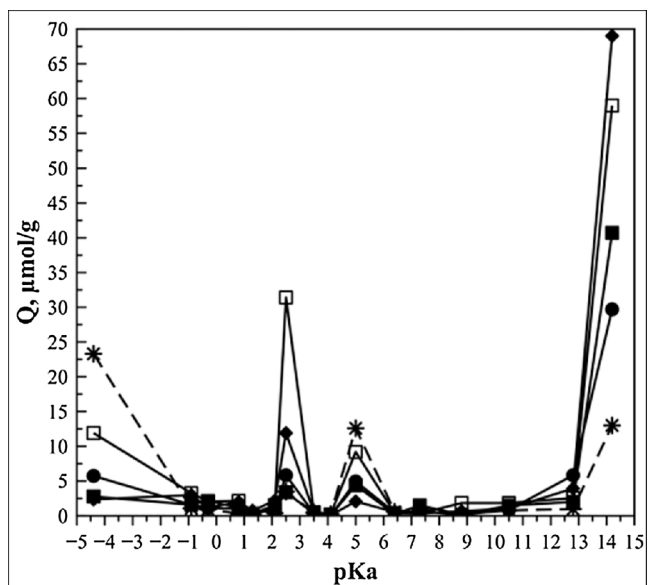


Fig. 11. Distribution of adsorption centers on the surfaces of ZrO_2 (*) and $\text{MoO}_3/\text{ZrO}_2$ obtained by impregnation (■, ◆) and dry mixing (□, ◇) from HPMo (■, □) and NHMO (●, ◆) and containing 4.2 wt.% MoO_3 .

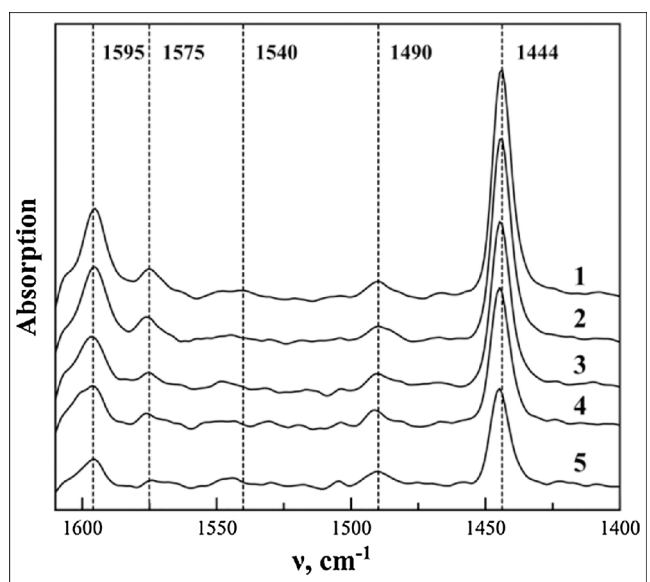


Fig. 12. IR spectra of adsorbed pyridine on $\text{MoO}_3/\text{ZrO}_2$ obtained by impregnation with NHMO and containing 4.2 wt.% MoO_3 at desorption temperature T_{des} ($^\circ\text{C}$): 20 (1); 150 (2); 200 (3); 250 (4) and 350 (5).

discussed below.

Calculations of pyridine concentration following [20] for the samples obtained by impregnation (Fig. 13) showed that the highest concentration of LAS was achieved in the case of ammonium paramolybdate as a precursor. Interestingly enough, compared to dry mixing, for 4.2NHMo(I) and 4.2HPMo(I) catalysts treated at 600°C there was a substantial amount of strong LAS, from which pyridine is not completely desorbed even at 350°C . This could be probably related to an increase of the t-ZrO₂ fraction for $\text{MoO}_3/\text{ZrO}_2$ catalysts made by impregnation (4.2 wt% MoO₃), because an increase of Lewis acidity is related to the content of t-ZrO₂ ($T = 600^\circ\text{C}$): $\text{NHMo(D)} \approx \text{HPMo(D)} \approx \text{HSiMo(D)} < \text{HPMo(I)} < \text{NHMo(I)}$ (Fig. 14, $T_{\text{des}} = 150^\circ\text{C}$).

The exact origin of Lewis acidity of the surface and its relationship with the phase composition are not completely clear requiring a further investigation. It was shown in [9] that modification of ZrO_2 made from

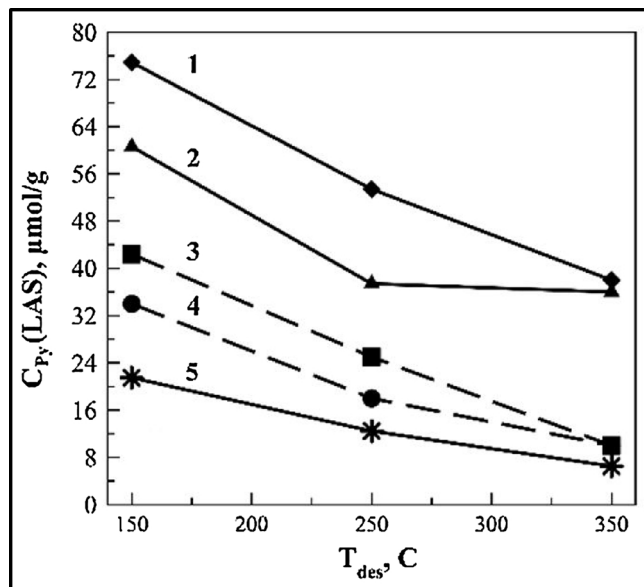


Fig. 13. Changes in the concentration of adsorbed pyridine on LAS of $\text{MoO}_3/\text{ZrO}_2$ with 4.2 wt.% MoO_3 obtained by impregnation (1, 2) or mixing (3, 4) from NHMo (1, 4), HPMo (2, 3) and $\text{ZrO}_2\text{-}600$ (5) as a function of desorption temperature.

$\text{Zr}(\text{OH})_4$ by molybdenum oxide (5 wt.% MoO_3 from NHMo) results in formation of specific LAS because of $\text{Zr}-\text{O}-\text{Mo}$ bonds formation on the catalyst surface near Zr^{4+} , which is reflected on the frequency of pyridine adsorption on LAS (type 19b with 1450 cm^{-1}). This suggestion is further confirmed by XRF done in [9] revealing presence of zirconium molybdate phase after thermal treatment at 820°C . In the current work, the same effect was not observed which can point out on modification of ZrO_2 surface by molybdenum oxide using impregnation at this treatment temperature (600°C). It should be noted that not only t- ZrO_2 can possess Lewis acidity. For instance, Ruslan et al. [9], as well as Morterra et al. [37] using FTIR of adsorbed 2,6-dimethylpyridine clearly showed presence of Lewis centers on the surface of m- ZrO_2 even if they were weaker than for t- ZrO_2 . Probably, t- ZrO_2 is responsible for strong adsorption of the probe molecules, i.e. the strong and medium strong sites are mainly located on the surface of t- ZrO_2 , while m- ZrO_2 exhibits weak Lewis acid sites. Experimental data given in Figs. 13 and 14 indirectly support the conclusions of [37] that t- ZrO_2 is responsible for formation of strong Lewis acids sites. It can be, however, stated that

Lewis centers *per se* are coordinatively unsaturated surface atoms of Zr^{4+} and for each modification of ZrO_2 the degree in such unsaturation is different.

For the catalysts made by dry mixing and thermally treated at 600°C there was almost no strong LAS; while concentration of the weak LAS was significant (Fig. 15). With an increase of MoO_3 there was a clear increase of BAS (Fig. 15b) in agreement with a substantial increase of overall surface acidity (Fig. 8), therefore Brønsted acidity of $\text{MoO}_3/\text{ZrO}_2$ catalysts made by dry mixing depends predominantly on MoO_3 amount. It should be noted that for determination of BAS recording of IR spectra was done directly at the desorption temperature without cooling, taking into account the background spectra at each temperature. This method giving the same results for Lewis acidity as the procedure with intermediate cooling, was found more reliable in elucidating the strength of BAS.

In addition to an increase of Brønsted acidity with an increase of molybdenum oxide content there was a decrease in the concentration of Lewis acid sites, which is clearly seen by relating the amount of pyridine on such sites calculated taking into account the specific surface area (Fig. 16B). A decrease in the concentration of LAS can be explained by a lower content of ZrO_2 , potential covering of molybdenum oxide by zirconia as well as lower Lewis acidity of molybdenum oxide *per se* not exceeding acidity of zirconia. Alternatively, in the catalyst used in the current work the Lewis acidity of molybdenum oxide might not be manifested because the well crystallized phase and subsequently coordinatively unsaturated Mo^{6+} are almost absent.

A sharp increase of Brønsted acid sites up to 6.6 wt.% speaks in favour of a molybdenum oxide monolayer formation on zirconia discussed above in section 3.3., while deceleration of an increase in the concentration of BAS with elevation of MoO_3 content from 6.6 to 13.2 wt.% is in line with titration data in the presence of Hammett indicators (Fig. 8).

Finally the acid strength distribution of acid centra in XHSiMo(D)-600 should be discussed (Table 5). As already mentioned above an increase of MoO_3 content leads to an overall decrease of the LAS. At the same time it follows from Table 5 that mainly strong LAS disappear while the amount of weak and medium LAS is even increasing. When the overall concentration of LAS is decreasing, the amount of BAS and the B:L ratio are increasing with elevation of MoO_3 content. At the same time the amount of strong BAS increased exceeding the total amount of weak and medium strong BAS.

Physico-chemical measurements allowed to establish clear correlations between the preparation methods and the structure of $\text{MoO}_3/\text{ZrO}_2$

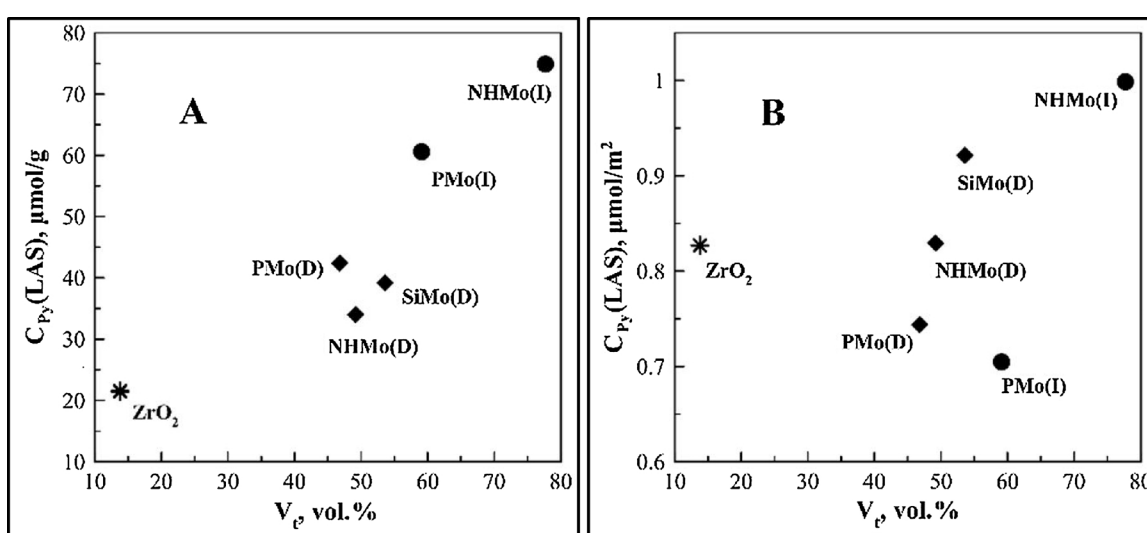


Fig. 14. Correlation between volume fraction t- ZrO_2 and LAS concentration at 150°C (A: μmol pyridine per g of catalyst; B: μmol pyridine per specific surface area) for samples with 4.2% MoO_3 obtained by impregnation (I) or mixing (D).

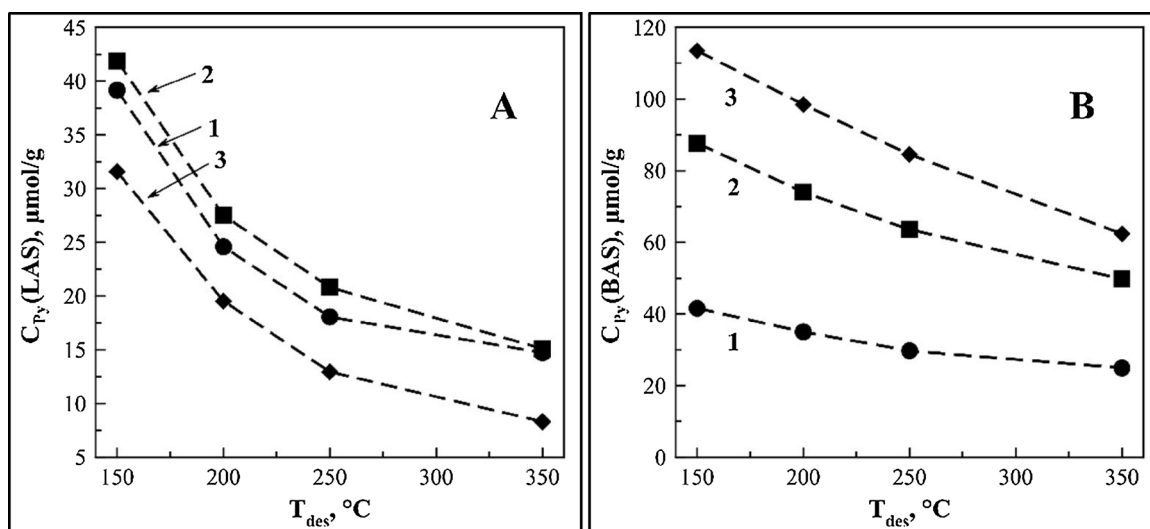


Fig. 15. Concentration of adsorbed pyridine on LAS (A) and BAS (B) on $\text{MoO}_3/\text{ZrO}_2$ obtained by mixing from HSiMo and containing 4.2 wt.% (1); 6.6. (2) and 13.2 (3) wt.% MoO_3 as a function of desorption temperature.

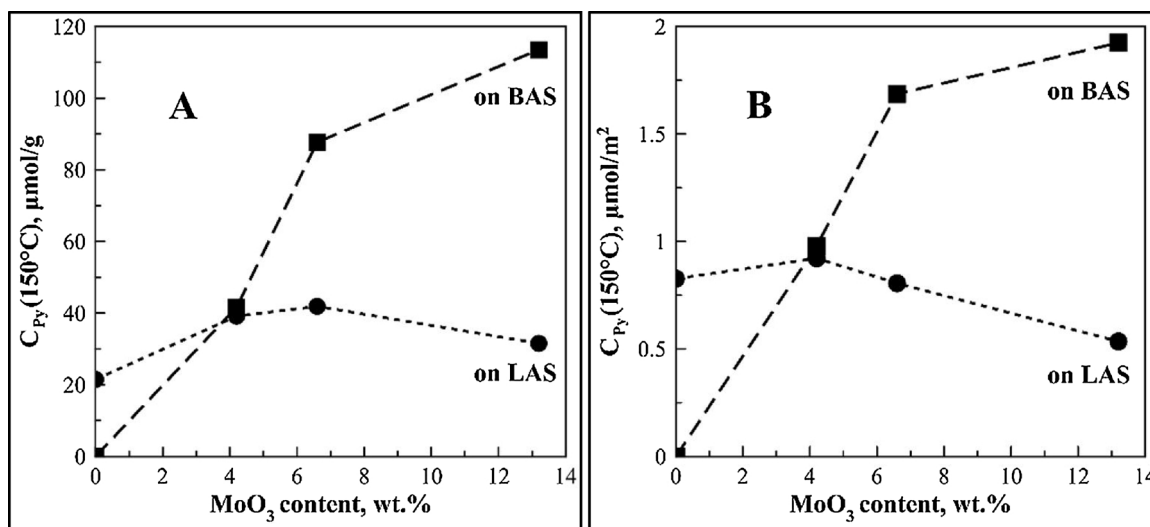


Fig. 16. Concentration of LAS and BAS as a function of MoO_3 content ($T_{des} = 150^{\circ}\text{C}$) (A: per gram of catalyst; B: per specific surface area).

catalysts. An increase of MoO_3 content (at the same thermal treatment temperature) slows down the phase transformation from a metastable t- ZrO_2 phase into a more stable m- ZrO_2 , which is reflected in a rise of the bulk concentration of t- ZrO_2 . This is accompanied by substantial changes in the porous structure of $\text{MoO}_3/\text{ZrO}_2$ catalysts, namely in the increase of the specific surface area and narrowing of the pore size distribution in favour of smaller size mesopores. The content of MoO_3 influences not only the bulk, but also the surface properties, in particular acidity. A substantial increase of acidity was noticed up to 6.6 wt. % MoO_3 along with a slight decrease of Lewis acidity. The latter is attribute to presence of zirconia while molybdenum oxide is responsible

for BAS. A strong dependence of acidity in this concentration domain is related to formation of a molybdenum oxide “monolayer” on the surface of zirconia because of the solid state wetting (SSW) [29,32], taking place in the current case already at 600°C . An analogous behaviour of the $\text{MoO}_3/\text{ZrO}_2$ system was reported by Chary et al. [34] when MoO_3 was introduced on ZrO_2 support by impregnation. This points out on some similarities for formation of $\text{MoO}_3/\text{ZrO}_2$ structure in the cases when there are no interactions between MoO_3 or its precursor and zirconium hydroxide at temperatures below crystallization of amorphous ZrO_2 .

The characteristics of $\text{MoO}_3/\text{ZrO}_2$ catalysts mentioned above

Table 5
The distribution of acid sites with different strength and their ratio for HSiMo(D)-600 samples.

MoO_3 content, wt.%	LAS, $\mu\text{mol/g}^a$			BAS, $\mu\text{mol/g}^a$			B\L ratio
	Weak, 150–250 $^{\circ}\text{C}$	Medium, 250–350 $^{\circ}\text{C}$	Strong, > 350 $^{\circ}\text{C}$	Weak, 150–250 $^{\circ}\text{C}$	Medium, 250–350 $^{\circ}\text{C}$	Strong, > 350 $^{\circ}\text{C}$	
4.2	21.1 (28.5)	3.3 (11.5)	14.7 (60.0)	11.9 (53.9)	4.8 (8.5)	24.9 (37.6)	1.06
6.6	21.1 (26.0)	5.7 (16.5)	15.1 (57.5)	24.1 (50.3)	13.9 (13.7)	49.7 (36.0)	2.10
13.2	18.6 (24.7)	4.6 (20.0)	8.3 (55.3)	27.4 (59.0)	22.1 (14.7)	61.4 (26.3)	3.51

^a In parenthesis (the relative amount in % compared to total BAS or total LAS respectively).

depend on the preparation method. The catalyst composition does not influence, however, only physico-chemical properties, but is also critical for catalytic activity as will be elucidated in the subsequent section.

3.5. Catalytic tests

In general, for alkylation of isobutane with butenes acid catalysts with different nature of acid sites have been utilized. It was pointed out [2,38] that the strength and concentration of LAS is decisive because they are involved in hydride transfer activating isobutane. A somewhat alternative opinion expressed in [39] suggests that not only LAS but also BAS are required for catalytic activity and moreover the ratio between BAS to LAS should be above 1.4. For alkanes isomerization on WO_3/ZrO_2 the optimum ratio of strong Brønsted to strong Lewis acid sites was reported to be equal to unity [40,41]. In order to resolve this controversy catalytic tests were performed with the samples possessing acid sites with different BAS/LAS ratios. Namely catalysts made by dry mixing with HSiMo as a precursor were selected as they display the most promising characteristics from the viewpoint of phase composition, pore structure and surface acidity.

3.5.1. Activity and selectivity

The catalytic performance of the three catalysts with different MoO_3 content as a function of time-on-stream is summarized in Fig. 17. For the sake of comparison this Figure also contains activity and selectivity data for the sulphated zirconia catalyst reported previously [42]. Table 6 contains the data on the product distribution for the same catalysts containing MoO_3 as well as for the reference catalyst.

The calculation of selectivity in alkylation and dimerization was done taking into account that 1-butene and 2-butene can take part in these reactions.

Data in Table 6 show that an increase of MoO_3 content leads to higher 1-butene conversion as well as selectivity in alkylation and dimerization of butenes. Comparison of the catalytic behaviour for materials with 4.2 and 6.6% MoO_3 reveals despite some similarities there

are also clear differences in selectivity. Both catalysts display a lower content of 2-butene (Fig. 17b) and minor cracking ability (Fig. 17e) with elevated selectivity in alkylation and dimerization. At the same time alkylation selectivity (Fig. 17d) does not differ that much for these samples, while a change in dimerization selectivity was substantial (Fig. 17c) increasing from 26.5 (4.2% MoO_3) to 35.6% (6.6% MoO_3). A further increase in MoO_3 to 13.2% promoted a significant increase of 1-butene conversion and alkylation selectivity, as well as isomerization of 1-butene by double bond migration giving 2-butenes.

The alkylate (Table 6) mainly consists of the C_8 fraction, comprising olefins (butene dimerization products) and dimethylhexanes (products of isobutane alkylation by butenes). With TOS there is a clear positive trend towards formation of olefins because of the dimerization reaction and formation of less alkylation products.

3.5.2. Catalytic properties and surface acidity

Comparing activity and selectivity of the catalysts with their physico-chemical properties the following correlations could be established. An increase in the content of MoO_3 leads to an increase of acidity (amount of BAS, Fig. 16), as well as an increase of 1-butene conversion (Fig. 17a) at every TOS, which is clearly visible from Fig. 18a. Concomitant with an increase of 1-butene conversion and Brønsted acidity, an increase of MoO_3 content results in a larger content of 2-butene (Fig. 18b). Comparison of selectivity along different reaction routes (alkylation, dimerization, oligomerization and isomerization) with acidity allows to conclude that Brønsted acidity is mainly responsible for changes in selectivity.

Different opinions can be found in the literature regarding the nature of acid sites responsible for isobutane alkylation. Feller et al. [39] and Stöcker et al. [43] pointed out on the prevalent role of strong BAS in controlling oligomerization for the liquid phase processes. At the same time other authors suggested that Bronsted sites with an intermediate strength are catalytically active [44]. An agreement, however, exists that very weak BAS acid sites only catalyze oligomerization [45]. Lavrenov et al. [2] and Paukshtis et al. [38] discussing ZrO_2 -containing systems argued that BAS play a negative role in alkylation. Satoh et al.

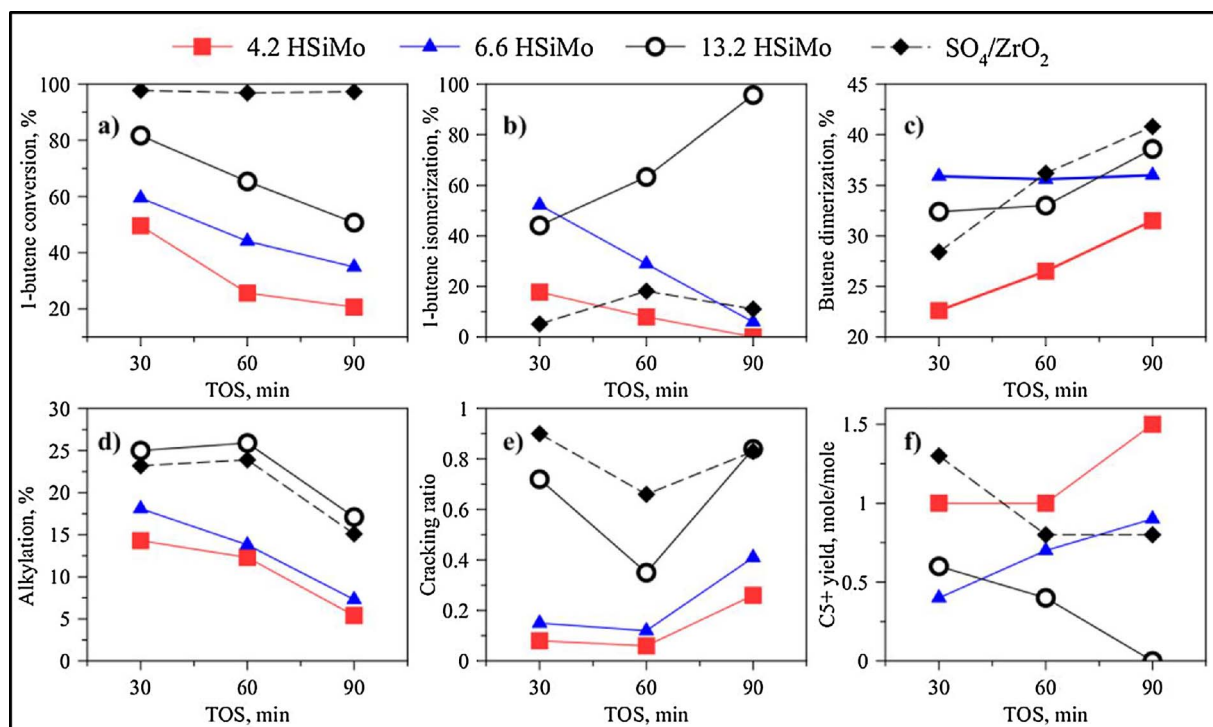


Fig. 17. Time on stream behaviour of HSiMo(D)-600 catalysts. a) 1-butene conversion; b) selectivity for isomerization, c): dimerization selectivity, d): alkylation selectivity; e) cracking ratio; f) mass yield of C_{5+} as % of olefin input.

Table 6

Molar compositions of alkylates obtained at different time on stream.

Catalyst	$\text{SO}_4^{2-}/\text{ZrO}_2$	4.2 HSiMo(D)	6.6 HSiMo(D)	13.2 HSiMo(D)
TOS, min	30	90	30	90
C_5	4.6	0.6	0.5	0.9
C_6	3.0	0.5	0.3	0.7
C_7	5.3	5.3	1.4	6.2
C_8	72.9	86.0	72.1	85.3
icl. TMP ^a	4.6	1.1	1.4	0.4
icl. DMH ^b	24.3	7.3	18.6	25.2
icl. MH ^c	1.7	13.2	6.5	1.2
icl. Olefines	40.1	62.8	44.2	56.7
Heavy end	14.2	7.7	25.7	12.8

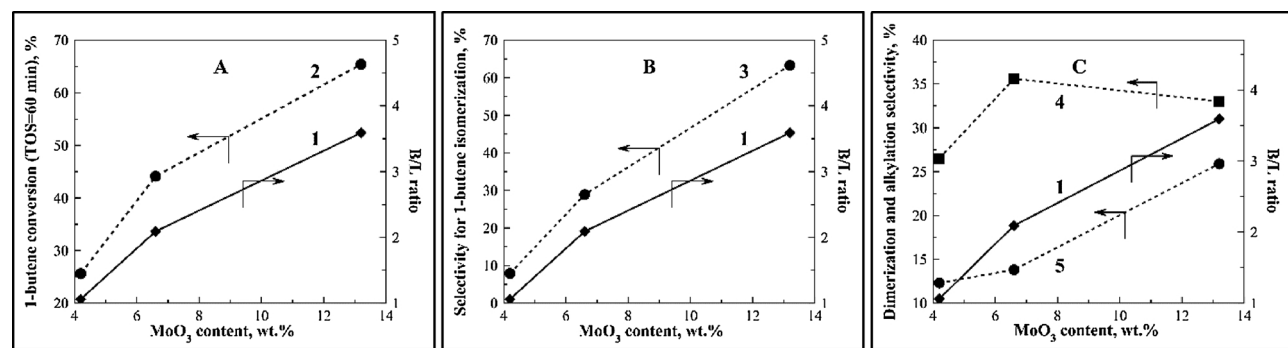
^a Trimethylpentanes.^b Dimethylhexanes.^c Methylheptanes.

Fig. 18. Correlation between 1-butene conversion (A, 2), selectivity in 1-butene isomerization (B, 3), dimerization (C, 4) and alkylation (C, 5) with acidity B/L (1) and the catalyst composition for TOS = 60 min.

[47] mentioned an important role of LAS in activation of isobutane and their subsequent alkylation with butenes in the gas phase process. However, the mechanism of alkylation is very complex and cannot be explained only by the presence on the surface of one type of acid sites, responsible for all reaction steps.

An often used in the literature descriptor for the surface acidity is the B/L ratio, taking into account presence of both types of sites. In a similar fashion the current work also contains comparison of B/L ratio, activity and selectivity with MoO₃ content in the catalyst (Fig. 18). As mentioned above in the literature the optimum ratio between BAS and LAS for alkylation is considered to be in the range between 1 and 1.4. Worth noting is the ratio B/L sites for 4.2% MoO₃ (Fig. 18), which is close to the optimal values of 1-1.4. An increase of B/L ratio up to 2 for the sample with 6.6% MoO₃ already results in lower selectivity towards alkylation, appearance of C₅₊ hydrocarbons and 2-butene. The experimental data are supporting the concept that an optimum ratio between BAS and LAS is needed for selective alkylation. However, while conversion and selectivity in 1-butene isomerization clearly correlate with an increase of B/L ratio which can be explained by activation of butenes on BAS, selectivity in alkylation and dimerization has a more complex behaviour depending on MoO₃ content and B/L ratio. Such behaviour clearly points out on importance of both types of active sites for surface reactions.

Kumar et al. [17] demonstrated for H- β zeolite and mesoporous MCM-41 that the porous structure and the strength of the Brønsted acid sites are responsible for selectivity in butene dimerization. In particular, presence of strong BAS and the microporous structure of H- β resulted in oligomerization and subsequent cracking, while selective dimerization with formation of C₈⁼ can be achieved in the case of weak BAS and the mesoporous structure (MCM-41). At the same time Zhang et al. [46] showed for H₄SiW₁₂O₄₀/SiO₂ that selective dimerization of n-butenes to C₈⁼ requires presence of strong BAS on the catalyst surface, suggesting that the reaction mechanism includes formation of an

energetically unfavorable secondary carbenium ion. Based on the data for the porous structure (Table 3), acidity (Fig. 16, Table 5) and catalytic behaviour (Fig. 18) it can be seen that an increase in MoO₃ content results in narrowing of pore size distribution in favour of small mesopores, as well as in an increase of the overall number BAS including the strong, medium and weak ones. An increase of MoO₃ content to 6.6% increases slightly the dimerization selectivity, which is concomitant with an increase of the absolute and relative amounts of medium strength BAS, as well as with an increase with the absolute number of strong BAS (Table 5).

Thus, selectivity in alkylation and dimerization is high in those case when the surface of MoO₃/ZrO₂ catalytic systems contain both LAS and BAS at the B/L ratio not exceeding 2, and the coverage of zirconia by molybdenum oxide does not exceed a monolayer coverage (samples with 4.2 or 6.6% MoO₃). Isomerization of 1-butene prevails over alkylation and dimerization for the sample having the coverage of molybdenum oxide exceeding the monolayer and the highest content of BAS.

Isomerization of butene-1 to butene-2 mainly visible upon increase of MoO₃ to 13.2% deserves a special discussion. From the thermodynamic viewpoint in an equilibrium mixture of C₄⁼ at low T the most prominent compound is isobutene [48]. At the same time because of kinetic limitations such equilibrium composition is often not reached for many catalysts. The mechanism of isomerization can be different [49,50] with the reaction proceeding on both BAS and LAS. A large number of studies was devoted to isomerization of butenes over MoO₃-containing catalysts [51–55]. Even zirconia can be active in this reaction [56–59]. Because of different types of catalysts and testing conditions 1-butene isomerization can proceed either to butene-2 by double bond migration or to isobutene by skeletal isomerization. Analysis of catalytic results and acidity points out on a linear correlation between selectivity in butene isomerization and B/L ratio. This suggests that in the conditions of the current work isomerization of butene-1 occurs on

Table 7
Thermogravimetrical analysis of spent catalysts.

Sample	Mass loss, %
4.2 HSiMo(D)	0.57
6.6 HSiMo(D)	0.66
13.2 HSiMo(D)	1.03
SO ₄ /ZrO ₂	2.98

BAS resulting in double bond migration rather than skeletal isomerization to isobutene.

In addition to the reactions mentioned above MoO₃/ZrO₂ systems promote also cracking of the products formed in dimerization/oligomerization and alkylation. The last section is thus related to cracking and its role in explaining the experimental results generated in the current work.

3.5.3. Catalyst deactivation

As can be seen from Fig. 17 there was a clear increase of conversion with an increase of MoO₃ loading. All catalysts experienced substantial deactivation with about the same extent except the reference SO₄/ZrO₂ catalyst. The cracking ratio can be correlated with acidity as higher acidity resulted in larger amounts of C₅–C₇ products.

In fact catalyst deactivation during alkylation of isobutane by butenes on solid catalysts is a well-known feature observed for zeolites [39,60,61], and sulphated zirconia ZrO₂ [2,3,6,14,61]. Supported [62] and bulk [63] HPA show similar behaviour. Cracking is also present in dimerization/oligomerization of butenes and skeletal isomerization of n-butenes to isobutene [17,49–64]. In general, two mechanisms of deactivation can be envisaged: a decrease of the surface area because of coking and pore blocking and a significant decrease of acidity because of acid site poisoning through strong chemisorption.

Application of sulphated zirconia in comparison with zeolites results in lower amounts of coke. Thus 5.6 mass % of coke deposits were reported for HY-zeolite while the corresponding value for SO₄²⁻/ZrO₂ was just 0.22 wt.% [61]. For zeolites there is a clear correspondence between coke formation and activity in the main alkylation reaction. Somewhat similar conclusions as drawn in [61] can be made based on the experimental data of the current work. Fig. 17 displays that the most active and stable catalyst, namely SO₄²⁻/ZrO₂, exhibits the highest cracking ratio. For catalysts containing 4.2 and 6.6% MoO₃, which show some selectivity for alkylation, but less stable, the cracking ratio is lower than for SO₄²⁻/ZrO₂. TGA data for the spent catalysts (Table 7) are in line with the stability ranking. This table illustrates that the amount of coke is increasing with MoO₃ content, moreover the largest amount of coke was deposited on SO₄²⁻/ZrO₂.

As a consequence, the catalyst with 13.2% MoO₃ gives predominantly dimerization and oligomerization with a subsequent cracking of dimers and oligomers to n-butene on strong BAS. Guisnet et al. [49,50] showed that in the reaction of n-butene skeletal isomerization the mechanism of dimerization-cracking plays a key role being responsible for formation of various C₃–C₅ cracking products from dimers. A similar mechanism can be operative in the current case, accounting for the second pathway of 1-butene transformation to 2-butene in addition to the double bond migration.

4. Conclusion

For the first time MoO₃/ZrO₂ catalysts were synthesized using a dry mixing method from various precursors. Genesis of MoO₃/ZrO₂ catalysts prepared by dry mixing and for comparison by impregnation was studied by a range of physico-chemical methods to reveal the impact of Mo precursor, loading and thermal treatment temperature on the catalyst properties. Such approach allowed establishing dependence of the phase composition, pore structure and acid-base properties on the

synthesis parameters. An increase of MoO₃ content to 6.6 mass % not only leads to substantial changes in the characteristics of MoO₃/ZrO₂ systems, but is also accompanied with formation of a monolayer of molybdenum oxide on zirconia (5 Mo/nm²) as a result of solid state wetting (SSW). Generation of such monolayer during dry mixing synthesis happened at temperatures at least 100 °C lower than previously reported and did not depend on the MoO₃ precursor. Formation of the molybdenum oxide monolayer on zirconia effect directly the acidic properties of the materials, which then influences the catalytic behavior.

All tested MoO₃/ZrO₂ catalysts exhibited selectivity in alkylation, but somewhat lower than SO₄/ZrO₂. Catalytic testing demonstrated that an increase of MoO₃ content results in stronger dimerization/oligomerization and cracking ability of MoO₃/ZrO₂ catalysts. When the content of MoO₃ is low (below 4.2 wt.%) and the monolayer of MoO₃ on ZrO₂ is not formed, isobutane alkylation and dimerization of butenes are more prominent than oligomerization and cracking to 2-butenes. Above the monolayer coverage (13.2 wt.% MoO₃) mainly oligomerization of butenes and isobutanes proceeds with subsequent cracking to 2-butenes or direct migration of the double bond in 1-butene gives 2-butene. All above mentioned reactions take place at the monolayer coverage (6.6 wt.% MoO₃). At a higher content of MoO₃ isomerization of 1-butene to 2-butene prevails, while cracking of alkylation and dimerization products on strong BAS can be another pathway for formation of 2-butenes on MoO₃/ZrO₂ catalysts.

Behaviour of MoO₃/ZrO₂ catalysts in general is consistent with catalytic properties of zeolites and modified ZrO₂ containing catalysts, possessing at the same time less prominent properties of solid superacids. Application of MoO₃/ZrO₂ catalyst gives predominantly dimerization/oligomerization of butenes rather than alkylation of isobutane.

Acknowledgements

The work was performed as a part of the state contract awarded on the basis of a grant of the Government of the Russian Federation for support of scientific research conducted under the supervision of leading scientists at Russian institutions of higher education, research institutions of State Academies of Sciences and state research centra of the Russian Federation on March 19, 2014, No. 14.Z50.31.0013.

References

- [1] D.Yu. Murzin, Chemical Reaction Technology, DeGruyter, Berlin, 2015.
- [2] A.V. Lavrenov, E.V. Perelevskii, V.P. Finevich, V.I. Zaikovskii, E.A. Paukshtis, V.K. Duplyakin, B.S. Bal'zhinimaev, Alkylation of isobutane with butenes on sulfated zirconia catalysts, Russ. J. Appl. Chem. 76 (2003) 550–557.
- [3] A. Corma, A. Martinez, C. Martinez, The effect of sulfation conditions and activation temperature of sulfate-doped ZrO₂, TiO₂ and SnO₂ catalysts during isobutene/2-butene alkylation, Appl. Catal. A 144 (1996) 249–268.
- [4] K. Arata, Preparation of superacids by metal oxides for reactions of butanes and pentanes, Appl. Catal. A 146 (1996) 3–32.
- [5] E.A. Vlasov, S.V. Myakin, M.M. Sychov, A. Aho, A.Yu. Postnov, N.V. Mal'tseva, A.O. Dolgashev, Sh.O. Omarov, D.Yu. Murzin, On synthesis and characterization of sulfated alumina–zirconia catalysts for isobutene alkylation, Catal. Lett. 145 (2015) 1651–1659.
- [6] D. Debasish, D.K. Chakrabarty, Activity and regenerability of sulfated zirconia superacid catalysts in isobutene/1-butene alkylation, Energy Fuels 12 (1998) 109–114.
- [7] S. Triwahyono, A.A. Jalil, N.N. Ruslan, H.D. Setiabudi, N.H.N. Kamarudin, C₅–C₇ linear alkane hydroisomerization over MoO₃-ZrO₂ and Pt/MoO₃-ZrO₂ catalysts, J. Catal. 303 (2013) 50–59.
- [8] J.R. Sohn, S.H. Kwon, D.C. Shin, Spectroscopic studies on NiO supported on ZrO₂ modified with MoO₃ for ethylene dimerization, Appl. Catal. A 317 (2007) 216–225.
- [9] N.N. Ruslan, N.A. Fedzillah, A.H. Karim, A.A. Jalil, S. Triwahyono, IR study of active sites for n-heptane isomerization over MoO₃-ZrO₂, Appl. Catal. A 406 (2011) 102–112.
- [10] V.V. Brei, O.V. Melezhyk, S.V. Prudius, M.M. Levchuk, K.I. Patrylak, Superacid WO₃/ZrO₂ catalysts for isomerization of n-hexane and for nitration of benzene, Stud. Surf. Sci. Catal. 143 (2002) 387–395.
- [11] V.A. Shkurenok, M.D. Smolikov, S.S. Yablokova, D.I. Kiryanov, A.S. Belyi, E.A. Paukshtis, N.N. Leonteva, T.I. Gulyaeva, A.V. Shilova, V.A. Drozdov, Pt/WO₃/ZrO₂ catalysts for n-heptane isomerization, Procedia Eng. 113 (2015) 62–67.
- [12] J.C. Yori, C.L. Pieck, J.M. Parera, Alkane isomerization on MoO₃/ZrO₂ catalysts,

- Catal. Lett. 64 (2000) 141–146.
- [13] N.N. Tominina, A.A. Pimersin, I.K. Moiseev, Sulphide catalysts for hydrotreatment of oil fractions, Russ. Chem. J. 52 (2008) 41–52.
- [14] W. Sun, Z. Zhao, G. Guo, X. Ye, W. Wu, Study of the alkylation of isobutane with n-butene over WO_3/ZrO_2 strong solid acid. I. Effect of the preparation method, WO_3 loading, and calcination temperature, Ind. Eng. Chem. Res. 39 (2000) 3717–3725.
- [15] M. Scheithauer, K. Grasselli, H. Knözinger, Genesis and structure of WO_x/ZrO_2 solid acid catalysts, Langmuir 14 (1998) 3019–3029.
- [16] J.R. Sohn, M.Y. Park, Characterization of zirconia-supported tungsten oxide catalyst, Langmuir 14 (1998) 6140–6145.
- [17] N. Kumar, P. Mäki-Arvela, T. Yläsalmi, J. Villegas, T. Heikkila, A.-R. Leino, K. Kordas, T. Salmi, D.Yu. Murzin, Dimerization of 1-butene in liquid phase reaction: influence of structure, pore size and acidity of Beta zeolite and MCM-41 mesoporous material, Micropor. Mesopor. Mater. 142 (2012) 127–134.
- [18] H. Toraya, M. Yoshimura, S. Somiya, Calibration curve for quantitative analysis of the monoclinic-tetragonal ZrO_2 system by X-ray diffraction, J. Am. Chem. Soc. 67 (1948) 119–121.
- [19] E.A. Vlasov, A.P. Nechiporenko, A.N. Kudryashova, Study of the acid-base surface characteristics of pseudoboehmite aluminum hydroxide and oxide, Russ. J. Appl. Chem. 59 (1986) 689–692.
- [20] C.A. Emeis, Determination of integrated molar extinction coefficients for infrared absorption bands of pyridine adsorbed on solid acid catalysts, J. Catal. 141 (1993) 347–354.
- [21] J.R. Sohn, E.W. Chun, Y.I. Pae, Spectroscopic studies on ZrO_2 modified with MoO_3 and activity for acid catalysts, Bull. Korean Chem. Soc. 24 (2003) 1785–1792.
- [22] E. López-Salinas, J.G. Hernández-Cortéz, I. Schifter, E. Torres-García, J. Navarrete, A. Gutiérrez-Carrillo, T. López, P.P. Lottici, D. Bersani, Thermal stability of 12-tungstophosphoric acid supported on zirconia, Appl. Catal. A 193 (2000) 215–225.
- [23] B.M. Devassy, F. Lefebvre, S.B. Halligudi, Zirconia-supported 12-tungstophosphoric acid as a solid catalyst for the synthesis of linear alkyl benzenes, J. Catal. 231 (2005) 1–10.
- [24] B.M. Devassy, S.B. Halligudi, Zirconia-supported heteropoly acids: characterization and catalytic behavior in liquid-phase veratrole benzoylation, J. Catal. 235 (2005) 313–323.
- [25] A.M.G. Pedrosa, D.M.A. Melo, M.J.B. Souza, A.S. Araujo, Synthesis, structure, and morphology of bifunctional catalysts based on zirconia modified by molybdenum oxide, J. Inorg. Mater. 44 (2008) 285–290.
- [26] P.D.L. Mercera, J.G. Van Ommen, E.B.M. Doesburg, A.J. Burggraaf, J.R.G. Ross, Zirconia as a support for catalysts. Evolution of the texture and structure on calcination in air, Appl. Catal. 57 (1990) 127–148.
- [27] E.A. El-Sharkavy, A.S. Khder, A.I. Ahmed, Structural characterization and catalytic activity of molybdenum oxide supported zirconia catalyst, Micropor. Mesopor. Mater. 102 (2007) 128–137.
- [28] M. Misono, Heterogeneous catalysis by heteropoly compounds of molybdenum and tungsten, Catal. Lett. 29 (1987) 269–321.
- [29] P. Afanasiev, On the metastability of ‘monolayer coverage’ in the $\text{MoO}_3/\text{ZrO}_2$ dispersion, Mater. Chem. Phys. 47 (1997) 231–238.
- [30] S.J. Gregg, K.S.W. Sing, Adsorption, Surface Area and Porosity, Acad. Press, London, 1982.
- [31] F. Prinetto, G. Cerrato, G. Ghiootti, A. Chiorino, Formation of the Mo^{VI} surface phase on $\text{MoO}_3/\text{ZrO}_2$ catalysts, J. Phys. Chem. 99 (1995) 5556–5567.
- [32] P. Afanasiev, C. Geantet, M. Breyssse, G. Coudrier, J.C. Vedrine, Influence of preparation method on the acidity of $\text{MoO}_3(\text{WO}_3)/\text{ZrO}_2$ catalysts, J. Chem. Soc. Faraday Trans. 90 (1994) 193–202.
- [33] K. Tanabe, M. Misono, Y. Ono, H. Hattori, New solid acids and bases and their catalytic properties, Stud. Surf. Sci. Catal. 51 (1989) 1–365.
- [34] K.V.R. Charly, K.R. Reddy, G. Kishan, J.W. Niemantsverdriet, G. Mestl, Structure and catalytic properties of molybdenum oxide catalysts supported on zirconia, J. Catal. 226 (2004) 283–291.
- [35] B. Zhao, X. Wang, H. Ma, Y. Tang, Raman spectroscopy studies on the structure of $\text{MoO}_3/\text{ZrO}_2$ solid superacid, J. Mol. Catal. A. 108 (1996) 167–174.
- [36] J. Xu, A. Zheng, J. Yang, Y. Su, J. Wang, D. Zeng, M. Zhang, C. Ye, F. Deng, Acidity of mesoporous $\text{MoO}_x/\text{ZrO}_2$ and WO_x/ZrO_2 materials: a combined solid-state NMR and theoretical calculation study, J. Phys. Chem. B. 110 (2006) 10662–10671.
- [37] C. Morterra, G. Meligrana, G. Cerrato, V. Solinas, E. Rombi, M.F. Sini, 2,6-dimethylpyridine adsorption on zirconia and sulfated zirconia systems. An FTIR and microcalorimetric study, Langmuir 19 (2003) 5344–5356.
- [38] E.A. Paukshtis, V.K. Duplyakin, V.P. Finevich, A.V. Lavrenov, V.L. Kirillov, L.I. Kuznetsova, V.A. Likholobov, B.S. Bal'zhinimaev, Mechanism of iso-butane alkylation by butenes over $\text{H}_3\text{PW}_{12}\text{O}_{40}$, $\text{H}_3\text{PTiW}_{11}\text{O}_{39}$, and Zr supported catalysts, Stud. Surf. Sci. Catal. 130 (2000) 2543–2548.
- [39] A. Feller, A. Gusman, I. Zuazo, J.A. Lercher, On the mechanism of catalyzed iso-butane/butane alkylation by zeolites, J. Catal. 224 (2004) 80–93.
- [40] W. Zhou, N. Soulantidis, H. Xu, M.S. Wong, M. Neurock, C.J. Kiely, I.E. Wachs, Nature of catalytically active sites in the supported WO_3/ZrO_2 solid acid system: a general perspective, ACS Catal. 7 (2017) 2181–2198.
- [41] D.C. Calabro, J.C. Vartuli, J.G. Santiesteban, The characterization of tungsten-oxide-modified zirconia supports for dual functional catalysis, Top. Catal. 18 (2002) 231–242.
- [42] S.Yu. Devyatkov, A.A. Zinnurova, A. Aho, D. Kronlund, J. Peltonen, N.V. Kuzichkin, N.V. Lisitsyn, D.Yu. Murzin, Shaping of sulphated zirconia catalysts by extrusion: understanding the role of binders, Ind. Eng. Chem. Res. 55 (2016) 6595–6606.
- [43] M. Stöcker, H. Mostad, A. Karlsson, H. Junggreen, B. Hustad, Isobutane/2-butene alkylation on dealuminated H EMIT and H FAU, Catal. Lett. 40 (1996) 51–58.
- [44] F.A. Diaz-Mendoza, L. Pernett-Bolano, N. Cardona-Martinez, Effect of catalyst deactivation on the acid properties of zeolites used for isobutane/butene alkylation, Thermochim. Acta 312 (1998) 47–61.
- [45] A. Feller, I. Zuazo, A. Guzman, J.O. Barth, J.A. Lercher, Deactivation pathways of zeolites in isobutane/butene alkylation, J. Catal. 216 (2003) 313–323.
- [46] J. Zhang, R. Ohnishi, T. Okuhara, Y. Kamiya, Preferential oligomerization of iso-butene in mixtures of isobutene and 1-butene over 12-tungstosilicic acid supported on silica, Appl. Catal. A 353 (2009) 68–73.
- [47] K. Satoh, H. Matsuhashi, K. Arata, Alkylation to form trimethylpentanes from isobutane and 1-butene catalyzed by solid superacids of sulfated metal oxides, Appl. Catal. A 189 (1999) 35–43.
- [48] A.V. Lavrenov, N.M. Ostrovskii, Yu.K. Demanov, Thermodynamics of isomerization of butylenes: equilibrium compositions, Pet. Chem. 41 (2001) 126–130.
- [49] M. Guisnet, P. Andy, N.S. Gnep, E. Benazzi, C. Travers, Selective skeletal butene isomerization through a bimolecular mechanism, Oil Gas Sci. Technol. 54 (1999) 23–28.
- [50] M. Guisnet, P. Andy, N.S. Gnep, E. Benazzi, C. Travers, Skeletal isomerization of n-butenes, I. Mechanism of n-butene transformation on a nondeactivated H-ferrite catalysts, J. Catal. 158 (1996) 551–560.
- [51] K. Nakamura, K. Eda, S. Hasegawa, N. Sotani, Reactivity for isomerization of 1-butene on the mixed $\text{MoO}_3\text{-ZnO}$ oxide catalyst, Appl. Catal. A 178 (1999) 167–176.
- [52] Y.-K. Park, S.J. Kim, N. You, J. Cho, S.J. Lee, J.H. Lee, J.-K. Jeon, $\text{MoO}_3/\text{SiO}_2$ catalysts for double bond migration of 2-butene, J. Ind. Eng. Chem. 17 (2011) 186–190.
- [53] J.G. Kim, Morphological change of $\text{Pt}/\text{MoO}_3/\text{SiO}_2$ for the synthesis of i-butylene from n-butene, J. Korean Ind. Eng. Chem. 7 (1996) 861–868.
- [54] S. Huang, H. Liu, L. Zhang, S. Liu, W. Xin, X. Li, S. Xie, L. Xu, Effects of acid leaching post-treatment on the catalytic performance of $\text{MoO}_3/\text{mordenite-alumina}$ catalysts for 1-butene metathesis reaction, Appl. Catal. A 404 (2011) 113–119.
- [55] T. Jin, H. Hattori, K. Tanabe, The $\text{MoO}_3\text{-SnO}_2$ catalysts. Acid-base properties and catalytic activities for 2-butanol decomposition and 1-butene isomerization, Bull. Chem. Soc. Jpn. 55 (1982) 2279–2280.
- [56] T. Yamaguchi, H. Sasaki, K. Tanabe, High selectivities of zirconium oxide catalyst for isomerization of 1-butene and dehydration of sec-butanol, Chem. Lett. 2 (1973) 1017–1018.
- [57] K. Tanabe, Surface and catalytic properties of ZrO_2 , Mater. Chem. Phys. 13 (1985) 347–364.
- [58] A. Ozake, K. Kimura, The effective site on acid catalysts revealed in n-butene isomerization, J. Catal. 3 (1964) 395–405.
- [59] Y. Nakano, T. Iizuka, H. Hattori, K. Tanabe, Surface properties of zirconium oxide and its catalytic activity for isomerization of 1-butene, J. Catal. 57 (1979) 1–10.
- [60] A. Feller, J.-O. Barth, A. Gusman, I. Zuazo, J.A. Lercher, Deactivation pathways in zeolite-catalyzed isobutane/butene alkylation, J. Catal. 220 (2003) 192–206.
- [61] C.A. Querini, E. Roa, Deactivation of solid acid catalysts during isobutane alkylation with C4 olefins, Appl. Catal. A 163 (1997) 199–215.
- [62] W. Chu, Z. Zhao, W. Sun, X. Ye, Y. Wu, Isobutane/butene alkylation over supported heteropoly acid catalysts: I. Influence of the structure of silica, Catal. Lett. 55 (1998) 57–61.
- [63] A. Corma, Martinez A, C. Martinez, Acidic Cs^+ , NH_4^+ , and K^+ salts of 12-tungstophosphoric acid as solid catalysts for isobutane/2-butene alkylation, J. Catal. 164 (1996) 422–432.
- [64] Yu.P. Khitev, I.I. Ivanova, Yu.G. Kolyagin, O.A. Ponomareva, Skeletal isomerization of 1-butene over micro/mesoporous materials based on FER zeolite, Appl. Catal. A 441–442 (2012) 124–135.